JCI The Journal of Clinical Investigation

MicroRNA-26a-3p rescues depression-like behaviors in male rats via preventing hippocampal neuronal anomalies

Ye Li, … , Wenjing Wang, Shu Yan Yu

J Clin Invest. 2021. https://doi.org/10.1172/JCI148853.

Research In-Press Preview **Neuroscience**

Graphical abstract

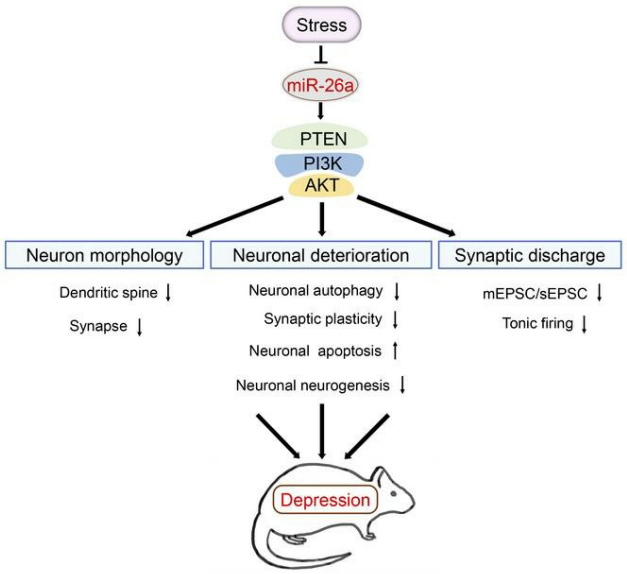

MicroRNA-26a-3p rescues depression-like behaviors in male rats via preventing hippocampal neuronal anomalies

Ye Li [1], Cuiqin Fan[1], Liyan Wang[2], Tian Lan[1], Rui Gao[3], Wenjing Wang[1], Shu Yan Yu[1, 4] *

1. Department of Physiology, School of Basic Medical Sciences, Cheeloo College of Medicine, Shandong University, Jinan, Shandong, 250012, China;
2. Morphological experimental center, School of Basic Medical Sciences, Cheeloo College of Medicine, Shandong University, Jinan, Shandong, 250012, China;
3. Department of Microorganism, Jinan Nursing Vocational College, Lvyoulu Road, Jinan, Shandong Province, 250012, PR China;
4. Shandong Key Laboratory of Mental Disorders, School of Basic Medical Sciences, Cheeloo College of Medicine, Shandong University, Jinan, Shandong, 250012, China;

* Corresponding author: Shu Yan Yu,

E-mail address: shuyanyu@sdu.edu.cn

Tel: +86-0531-88383902

Abstract

Depression is a neuropsychiatric disease associated with neuronal anomalies within specific brain regions. In the present study, we screened microRNA (miRNA) expression profiles in the dentate gyrus (DG) of hippocampus and found miR-26a-3p was markedly down-regulated in the rat model of depression, whereas up-regulation of miR-26a-3p within DG regions rescued the neuronal deterioration and depression-like phenotypes resulting from stress exposure, effects which appear to be mediated by the PTEN pathway. The knock-down of miR-26a-3p in DG regions of normal control rats induced depression-like behaviors, effects which were accompanied with an activation of PTEN-PI3K/Akt signaling pathway and neuronal deterioration via suppression of autophagy, impairments in synaptic plasticity and the promotion of neuronal apoptosis. In conclusion, these results suggested that a miR-26a-3p deficits within the hippocampal DG mediated the neuronal anomalies contributing to the display of depression-like behaviors. This miRNA may serve as a potential therapeutic target for the treatment of depression.

Keywords： miR-26a-3p; neuronal anomalies; hippocampus; PTEN; Depression

Introduction

Depression is a prevalent psychiatric disorder related to structural and functional neuronal changes within specific brain regions (1-3). Currently, most clinical treatments for depression have focused on restoring dysregulated monoamine neurotransmitter systems within the brain (4, 5). However, the limited benefits associated with such treatments indicate that more complicated mechanisms are involved with the etiology of depression (6-8). Previous evidence from clinical studies have indicated that the disruptions in the normal structural and functional homeostasis in specific brain regions may involve in the progression of depression in patients (1, 9). Consistently, accumulating results from animal models of depression have indicated that stressful stimuli produce neuronal injury for example the increased apoptosis within the hippocampus or medial prefrontal cortex, and thus resulted in the display of depression-like behaviors (10-13). However, details regarding the mechanisms of these neurological processes involved in the pathological damage in depression are not fully understood. Therefore, it is necessary to achieve a more comprehensive identification of potential molecular targets and novel pathways underlying the genesis and development of depression.

Recent genomic studies have revealed that dysregulated expressions within a broad spectrum of non-coding RNAs (ncRNAs) are implicated in various neurological diseases (14). MicroRNAs (miRNAs), as widespread and diverse endogenous ncRNAs that can

regulate gene expression by directly modifying messenger RNA (mRNA) after transcription (15), have attracted considerable attention of late due to their capacity to regulate neuronal development and function (16, 17). Through their ability to target and suppress endogenous mRNAs, miRNAs can inhibit the translation of proteins (18). Therefore, any disruption or imbalance in the expression and function of miRNA networks could lead to neurological diseases and, in fact, there is accumulating evidence that miRNAs have been implicated in neurological disorders such as Parkinson's disease (PD), Alzheimer's disease (AD) and major depression disorder (MDD) (19-21). Thus, expression changes in specific miRNAs could serve as potential biomarkers for diagnostic or therapeutic targets in clinical practice (22). However, the underlying mechanisms of miRNAs in contributing to the development and progression of these neurological disorders, in particular depression, remain largely unknown. Thus, the screening of specific miRNAs, their underlying mechanisms and possible downstream signaling pathways as related to a neuronal dysfunction associated with depression may provide new therapeutic strategies for the treatment of this condition.

In the present study, we examined the differentially expressed miRNA profile in a chronic unpredictable mild stress (CUMS)-induced rat model of depression versus normal controls using a high-throughput microarray. We found that miR-26a-3p, a potential miRNA that is responsible for regulation of mRNA-encoding proteins related to stress and

depression (23), showed a significant differential expression within the dentate gyrus (DG) hippocampus of CUMS versus control rats and interacted with the phosphate and tension homology deleted on chromsome ten (PTEN)-phosphoinositide 3-kinase (PI3K)/protein kinase B (Akt) signaling pathway. Complementing these findings, the knock-down of miR-26a-3p in DG regions of control rats accelerated neuronal deterioration and induced depression-like behaviors, whereas an up-regulation of miR-26a-3p within DG regions of CUMS-induced depressed rats rescued neuronal deterioration and depression-like phenotypes. Accordingly, these results provide novel insights into mechanisms involving the functional regulation of miRNAs in depression, and, in specific, identify miR-26a-3p as a new potential target for depression prognosis and therapy.

Results

Identification of differentially expressed miRNA profiles in the CUMS-induced rat model of depression

MiRNA expression profiles vary markedly as a function of different cell types and conditions. Therefore, we first investigated miRNA expression profiles within the DG hippocampus in normal control and CUMS-induced depressed rats using the Illumina HiSeq 2500 high-throughput sequencing (miRNA-seq) technique. Expression patterns of miRNAs were compared between depressed and normal rats with use of hierarchical

clustering analysis (Figure 1A). Differentially expressed miRNAs were displayed as fold change filtering (Figure 1B), with statistically significant differential changes in miRNAs between the two groups identified with use of volcano plot filtering (Figure 1C) and principal component analysis (PCA) plot (supplementary Figure 1). With this analysis, 57 miRNAs were detected to be significantly different between depressed and normal DG samples using the criteria of fold change $\geqslant$ 2.0 and $P < 0.05$ as the cutoff threshold. Among the differentially expressed miRNAs, 9 were up-regulated and 48 down-regulated in DG regions of depressed as compared with that of normal rats. These results demonstrate that clear differences are present in the differential expression of miRNAs in DG tissues between normal and depressed rats. Next, to validate miRNA-seq results for some of these miRNAs, levels of miR-26a-3p, miR-1298, miR-211-5p and miR-34b-3p in DG tissues, including the samples for sequencing analysis, were determined using qPCR. These four miRNAs showed significantly decreased levels within DG regions of CUMS-induced versus normal rats (Figure 1D). These results indicate that the qRT-PCR data were consistent with that of the miRNA-seq analysis regarding expression levels of these four miRNAs.

PTEN is a direct target gene of miR-26a-3p

To examine the functional effects of miRNAs, possible miRNAs associated with

depression-related pathways were assessed. With use of DIANA-miRPath, all candidate miRNAs involved in possible pathways, as identified using a p-value cutoff of 0.05, were determined. With this analysis, miR-26a-3p was recognized as showing the greatest potential for being implicated in neuronal related injury pathways, which could then be considered as contributing to the pathogenesis of depression. Therefore, we focused our investigation on miR-26a-3p, which was significantly decreased to the lowest levels as observed in the DG of these depressed rats. The predicted target genes of miR-26a-3p, as associated with neuronal regulatory pathways, were the examined using DIANA-miRPath (Figure 2A). The functional annotation data revealed that eight genes, which were significantly correlated with neuronal plasticity and development, could be regulated by miR-26a-3p (Figure 2B). Among these predicted target genes, *PTEN,* which contributes to cell development, migration and apoptosis, was considered as a crucial factor involved in mediating the regulatory effects of miR-26a-3p related to neuronal injury in depression. Therefore, to determine the molecular mechanisms of miR-26a-3p, a Dual-luciferase reporter assay was used to validate the direct target gene of miR-26a-3p. It was predicted that the 3'-UTR of PTEN mRNA would contain a putative binding site for the seed match sequence of miR-26a-3p (Figure 2C). Results of this assay demonstrated that miR-26a-3p significantly repressed reporter activity of the transcript containing the wild-type 3'-UTR of PTEN mRNA (by 0.32 $\pm$ 0.02-fold versus miR-NC, $P < 0.01$), indicating that miR-

26a-3p exerts a direct regulatory effect on PTEN (Figure 2D).

Knock-down of miR-26a-3p in the DG induces depression-like behaviors and decreased synaptic transmission in rats

Oligonucleotides against miR-26a-3p were cloned into the AAV virus vector (AAV-miR-26a-3p-sponge) to knock down miR-26a-3p expression and function in the DG of normal rats, while a vector included scramble sequence was constructed to serve as a negative control (Figure 3A and supplementary Figure 2). After bilateral stereotaxic infusion into the DG (Figure 3B, C), the knock-down efficiency of miR-26a-3p was examined with use of qRT-PCR and showed a 74% decrease in DG regions compared to the control group ($P < 0.01$), a similar trend like that observed in the CUMS-exposure group (Figure 3D). Particularly, significant was the observation of depression-like behaviors in these knock-down miR-26a-3p rats at 14-days post-infusion. Results from the sucrose preference test showed that knock-down of miR-26a-3p within the DG significantly decreased the consumption of sucrose as compared with rats receiving a mock control injection, results which provide an index of anhedonia (Figure 3E). Moreover, increased immobility and decreased swimming times in rats with a knock-down of miR-26a-3p was observed in the forced swimming test, responses indicative of behavioral despair in these rats (Figure 3F). In addition, results from the open field test showed that knock-down of miR-26a-3p have

no effects on the spontaneous locomotor activity of rats ($P > 0.05$, supplementary Figure 3). Next, whole-cell patch-clamp measures on neurons from DG coronal slices and miniature and spontaneous excitatory post-synaptic currents (EPSCs) were assessed in these rats. We found that, as compared with that of controls receiving the mock empty vector, the knock-down of miR-26a-3p inhibited both amplitudes and frequencies of mEPSCs and sEPSCs (Figures 3G, H) as well as spontaneous tonic firing (Figure 3I), effects similar to that observed in CUMS-exposure rats. These results suggest that a miR-26a-3p deficit inhibits synaptic transmission in DG pyramidal neurons in the hippocampal microcircuit, which may then contribute to the depression-like behaviors observed in rats.

Knock-down of miR-26a-3p increases PTEN expression and inhibits autophagy in rats

Results from western blot analysis showed that, in contrast to that observed in mock controls, the knock-down of miR-26a-3p increased protein levels of PTEN in the DG region, again findings which were similar to that of the increased expression levels of PTEN seen in rats following 5 weeks of CUMS-exposure (Figure 4A). Moreover, expressions of PI3K and phosphorylated Akt were significantly down-regulated, accompanied with an up-regulation of p53 in the miR-26a-3p knock-down group as compared with controls (Figure 4A). To further explore possible neuronal mechanisms of

miR-26a-3p in depression, we examined whether this miR-26a-3p-PTEN axis could modulate autophagy. We found that the knock-down of miR-26a-3p in DG regions also markedly down-regulated the LC3-II/I ratio and Beclin-1expression, while increasing the expression of p62 (Figure 4B). Meanwhile, images from electron microscopy revealed that the amount of autophagosomes in the DG region were significantly decreased (Figure 4C). These results demonstrate that PTEN is a target of miR-26a-3p and the up-regulation of PTEN expression by the knock-down of miR-26a-3p appears to result in suppression of autophagic activity within the DG.

Knock-down of miR-26a-3p induces dysregulation of neuronal plasticity in the DG

Results from our immunofluorescent analysis also showed that miR-26a-3p knock-down rats exhibited a significant decrease in key neuroplasticity-related markers, including synaptophysin (Syn) and postsynaptic density protein 95 (PSD-95) as compared with the mock controls (Figure 5A), and as well as microtubule-associated protein 2 (MAP-2) (supplementary Figure 4A, B). Results from our western blot analysis revealed that low-levels of expression in a series of neuroplasticity-related regulators within the DG were observed in response to miR-26a-3p knock-down as compared with that in mock control rats (Figure 5B). These findings from miR-26a-3p knock-down rats were similar to that found within the DG of our CUMS-induced rat model of depression. Moreover, mRNA

expression levels of these main neuroplasticity-related regulators in response to miR-26a-3p knock-down were similar to the tendencies of change in their protein expression levels (supplementary Figure 4C). Morphological examinations revealed that decreased numbers of synapses were present within DG regions in both miR-26a-3p knock-down and CUMS-induced depressed rats (supplementary Figure 4D). Dysregulation in neuroplasticity was further confirmed by the significant losses of dendritic spines observed in miR-26a-3p knock-down rats (Figure 5C).

Knock-down of miR-26a-3p promotes neuronal apoptosis in the DG

Results from immunofluorescence staining showed that cleaved Caspase-3, a terminal regulator that prompts the apoptosis process, was significantly increased (Figure 6A), while the neuronal precursor marker, Doublecortin X (DCX) (Figure 6A), and neural stem cell marker, Nestin (supplementary Figure 5A, B), were significantly decreased within DG regions of miR-26a-3p knock-down rats. Following miR-26a-3p knock-down significant increases in protein levels of the pro-apoptotic factors, Bax, caspase-3 and caspase-9, accompanied with decreased expression levels of Bcl-2 were observed within the DG as indicated from results of western blotting (Figure 6B). Similar trends were obtained with regard to transcriptional levels of these apoptosis-related factors (supplementary Figure 5C). Morphological changes as observed with Hoechst-33258 staining (supplementary

Figure 5D) and transmission electron microscopy (Figure 6C) demonstrated that the nuclei within DG neurons exhibited remarkable characteristics of apoptosis, including nuclear chromatin margination, aggregation and condensation in miR-26a-3p knock-down versus mock control rats. The number of apoptotic cells within DG areas were correspondingly increased after knock-down of miR-26a-3p. Interestingly, we consistently observed that these tendencies for apoptotic morphological changes and apoptotic-related factor expressions as observed in miR-26a-3p knock-down rats were also present in CUMS rats. These results provide further evidence implicating that a down-regulation of miR-26a-3p within the DG contributes to neuronal apoptosis which may then be responsible for the induction of neuronal injury and depression-like behaviors in rats.

Overexpression of miR-26a-3p in the DG rescues depression-like behaviors and impaired synaptic transmission in depressed rats

As a complementary approach to evaluate the role of miR-26a-3p in maintaining homeostasis and function of the DG neuronal network, an AAV- miR-26a-3p virus was infused into the DG region to overexpressed miR-26a-3p in CUMS rats (Figure 7A). A presentation of the experimental design is shown in Figure 7B. The infection efficiency of miR-26a-3p was examined with use of immunofluorescence (Figure 7C) and a significant increase in miR-26a-3p expression levels within isolated DG regions were observed in

miR-26a-3p overexpressed rats (Figure 7D). Interestingly, restoration of miR-26a-3p levels within the DG significantly ameliorated symptoms of anhedonia and behavioral despair resulting from 5-weeks of CUMS exposure, as evidenced by increases in sucrose consumption (Figure 7E) and decreases in immobility and increases in swimming times (Figure 7F) as compared to CUMS rats receiving the mock virus. However, results from the open field test showed that overexpression of miR-26a-3p within DG regions of CUMS rats have no effects on the spontaneous locomotor activity in rats ($P > 0.05$, supplementary Figure 6). We also found that overexpression of miR-26a-3p in CUMS rats significantly increased the amplitudes and frequencies of both miniature excitatory postsynaptic currents (mEPSCs) and spontaneous excitatory postsynaptic currents (sEPSCs) in DG pyramidal neurons (Figure 7G, H) as well as spontaneous tonic activity (Figure 7I) in the CUMS group. These findings suggest that restoration of abnormal excitatory synaptic activity in DG granule cells contributes to the amelioration of depression-like behavior in CUMS rats and that an up-regulation of miR-26a-3p within the DG rescues the core symptoms of depression in depressed rats.

Overexpression of miR-26a-3p suppresses PTEN expression and increases autophagy in depressed rats

Overexpression of miR-26a-3p within the DG significantly decreased protein expression

levels of PTEN, a direct target of miR-26a-3p, in depressed rats (Figure 8A), and the changes in protein levels of PI3K, phosphorylated Akt and p53 resulting from CUMS-exposure were also restored in response to the overexpression of miR-26a-3p within the DG. Moreover, we observed that an overexpression of miR-26a-3p increased levels of LC3II/I and Beclin-1 and decreased levels of p62 (Figure 8B). The expression changes in these autophagy-related proteins provide further support for the hypothesis that miR-26a-3p/PTEN pathway may rescues depression-like behaviors via regulating autophagic activity in depressed rats. Finally, electron microscopy images reveal the restoration in autophagy resulting from an up-regulation of miR-26a-3p within the DG of depressed rats (Figure 8C). Taken together, these results provide compelling evidence indicating that miR-26a-3p induces autophagy within the DG of depressed rats.

Overexpression of miR-26a-3p ameliorates the dysregulation of neuronal plasticity in depressed rats

Results from immunofluorescent analysis showed that the main synaptic markers, Syn, PSD-95 (Figure 9A) and MAP-2 (supplementary Figure 7A, B), were increased within the DG area following miR-26a-3p overexpression. Overexpression of miR-26a-3p as achieved with an AAV-miR-26a-3p virus infection markedly ameliorated the dysregulation of neuronal plasticity in depressed rats as evidenced by increased protein (Figure 9B) and

mRNA (supplementary Figure 7C) levels of plasticity-related mediators within the DG of depressed rats. Moreover, we observed that the overexpression of miR-26a-3p significantly restored the number of synapses (supplementary Figure 7D) and dendritic spine densities (Figure 9C) in DG neurons, which had been reduced by CUMS-exposure. These results provide convincing evidence that overexpression of miR-26a-3p ameliorated the dysregulation of neuroplasticity in depressed rats.

Overexpression of miR-26a-3p inhibits neuronal apoptosis in depressed rats

Compared with the non-stressed control group, CUMS rats displayed decreased expressions of the neurogenesis markers, DCX (Figure 10A) and Nestin (supplementary Figure 8A, B) along with increased protein (Figure 10B) and mRNA (supplementary Figure 8C) expression levels of pro-apoptotic factors within DG areas. All these changes, as observed in these depressed rats, were alleviated with an up-regulation of miR-26a-3p. Moreover, morphological results as obtained with Hoechst-33258 staining (supplementary Figure 8D) and transmission electron microscopy (Figure 10C) showed that an up-regulation of miR-26a-3p within the DG of depressed rats significantly restored the nuclear deterioration resulting from CUMS exposure. These results suggest that miR-26a-3p suppresses neuronal apoptosis and promotes neurogenesis within the DG area, effects which may work through the PTEN signaling pathway in depression.

PTEN mediates neuronal and behavioral anomalies resulting from miR-26a-3p deficits in the DG

Finally, to substantiate that the neuronal deterioration induced by miR-26a-3p was dependent on the PTEN signaling pathway, miR-26a-3p knock-down rats were treated with the PTEN inhibitor, BPV (pic). As shown in Figure 11A, BPV (pic) treatment (0.2 mg/kg, i.p.) decidedly up-regulated PI3K and induced Akt phosphorylation, two vital downstream components of the PTEN pathway that were significantly suppressed by miR-26a-3p knock-down in DG regions. BPV (pic) treatment also decreased the up-regulation of p53 resulting from this miR-26a-3p deficit as well as markedly up-regulating the LC3-II/I ratio and Beclin-1 and decreasing levels of p62 (Figure 11B), suggesting that inhibition of PTEN restored the autophagy suppressed by the miR-26a-3p deficit. In addition, BPV (pic) treatment up-regulated neuroplasticity-related mediators (Figure 11C) and reduced expressions of pro-apoptotic factors in miR-26a-3p knock-down rats (Figure 11D). These results demonstrated that this pharmacological inhibition of PTEN significantly reversed the neuronal deterioration and cell death resulting from miR-26a-3p knock-down. BPV (pic) treatment also effectively ameliorated the depression-like symptoms from this miR-26a-3p deficit as based upon results obtained with the sucrose preference (Figure 11E) and forced swim (Figure 11F) tests and reversed the decreases in frequencies of spontaneous

tonic firing (Figure 11G) in DG neurons of depressed rats.

Discussion

Despite accumulating evidence from increasing numbers of studies indicating a relationship between depression and neuronal anomalies in specific brain regions, effective antidepressant therapeutic strategies remain elusive (24, 25). Following exposure to CUMS, we found that the resultant depression-like symptoms were accompanied with significant structural and functional neuronal changes within hippocampal DG regions in rats. Previous results from our laboratory have indicated that the depression associated with chronic stress appears to result in neuronal apoptosis and aggravates dendritic spine impairments, while suppression of this neuronal deterioration promotes recovery from depressive behaviors in animal models of depression (26-28). However, details regarding the underlying mechanisms of these pathophysiological processes in depression are not fully understood. Thus, the potential for development of corresponding therapeutic measures targeting these mechanisms remain largely unknown. In this study, we identified differentially expressed miRNAs and assessed their functions with use of high-throughput sequencing and bioinformatic analysis in an animal model of depression. Notably, miR-26a-3p was found to be significantly down-regulated in hippocampal DG tissues of depressed rats, suggesting that this differentially expressed miRNA might play an

important role in the development and pathogenesis of depression (29). Previous studies from bioinformatical analysis predicted that miR-26a-3p involves numerous pathways, in particular pathways targeting some specific genes associated with the regulation of synaptic plasticity and development within the nervous system (30-32). Moreover, as revealed from results of luciferase reporter assays, the present study demonstrated that miR-26a-3p contains conserved seed matches to PTEN mRNA and expression levels of PTEN were decreased with an over-expression of miR-26a-3p, while the knock-down of miR-26a-3p reversed this reduction of PTEN as demonstrated *in vivo*. Therefore, these results suggest that miR-26a-3p might serve as a regulator in the development of depression. Previous studies have reported that miR-26a-2 possesses antidepressant efficacy by targeting autoreceptor HTR1A in serotonergic neurons (33). Meanwhile, PTEN was validated to act as a potential target of miR-26a in some cancer research (34-36). However, detailed mechanisms regarding the miR-26a-3p/PTEN dysregulation underlying the neurological damages, in particular whether this neuronal injury is involved in the pathogenesis of depression is unknown.

Recent studies have demonstrated that the depression associated with chronic stress was accompanied with dendritic remodeling in hippocampal neurons (37, 38). Notably, the brain-derived microRNAs could regulate dendritic spine development and may thus be involved in regulating neural plasticity and behaviors (39, 40). In order to further explore

functions of the miR-26a-3p/PTEN axes as related to depression, we utilized the CUMS-induced rat model of depression. Results showed that chronic stress produced specific changes in synaptic transmission within the hippocampal DG network of rats, consisting of reduced excitatory synaptic transmission as revealed from recordings of both mini EPSCs and spontaneous EPSCs along with reduced burst activity in DG pyramidal neurons. MiR-26a, a brain-enriched microRNA mainly localized within axonal compartments of neurons, has been hypothesized to play a key role in axon development and regeneration (41, 42), and also involved in the formation, maturation and/or plasticity of synapses via regulating distinct sets of target genes (43). For example, it has been suggested that miR-26a is involved in regulating excitatory neurotransmission under stress condition (44), and maintains stress resiliency and antidepressant efficacy by targeting the serotonergic autoreceptor (33). Therefore, these alterations in synaptic transmission found in the present study may be due to impaired neurobiological functions as correlated with miR-26a-3p deficits induced by stressors. In support of this conjecture we found that miR-26a-3p can reduce synaptic transmission failure, enhance autophagy-lysosomal activities, facilitate synaptic plasticity and suppress neural apoptosis. This capacity for miR-26a-3p to ameliorate synaptic transmission failure may be via an integration of specific neuronal networks participating in the rescue of specific brain dysfunctions related to depression phenotypes. In this way, activation of the miR-26a-3p pathway results in antidepressant

effects. Therefore, we hypothesized that neuronal anomalies resulting from chronic stress may be related with synaptic dysfunction in the hippocampal networks eventually leading to a depression-like state in rats. Interestingly, certain stressors not only produce general alterations in neuronal functions but also induce a specific reduction in miR-26a-3p expression, which appears to be a key factor acting upon specific neuronal circuits and regulating the activity of DG neurons in depression.

Based upon these findings, an over-expression of miR-26a-3p improved neurological function recovery along with reductions depression-like symptoms in CUMS rats provides persuasive evidence for this speculation. Meanwhile, to determine whether miR-26a-3p produces nonspecific response in the depression-like behavioral alterations, the locomotor activity of rats was measured by the open field test. The results showed that miR-26a-3p alterations within DG region have no effect on the spontaneous locomotor activity. Moreover, this over-expression of miR-26a-3p was associated with a down-regulation of PTEN expression and increases in PI3K and Akt phosphorylated levels. PI3K/Akt and p53 signaling are considered a possible downstream pathway of PTEN, which can then regulate cell functions (45, 46). Up-regulating PTEN accelerates the inactivation and degradation of phosphorylated PI3K, thereby restraining the PI3K/Akt pathway (47). While we were able to demonstrate the capacity for miR-26a-3p to target the inhibition of PTEN protein translation, the mechanisms for the antidepressant-like effects of this pathway remain

unclear. Based on the data obtained in the present study, along that in the literature, we propose that the restoration of synaptic transmission may involve an upregulation of brain-derived neurotrophic factor (BDNF) or synaptogenesis (48, 49). In addition, removal of damaged or dysfunctional proteins and organelles via enhancement of autophagy-lysosomal activities may, in turn, inhibit apoptosis pathways in neurons (50). Such neuroprotective processes can rebalance functioning of the hippocampal network and subsequently elicit antidepressant effects.

To directly address the issue of whether the PTEN-PI3K/Akt signaling pathway functionally contributes to stress vulnerability as a target of miR-26a-3pwe demonstrated that PTEN expression was up-regulated after knock-down of miR-26a-3p in DG regions. Then, BPV (pic), the antagonist of PTEN, was used to assess whether miR-26a-3p exerts antidepressant effects via suppression of the PTEN pathway (51-53). BPV (pic) significantly promoted autophagy, reduced apoptotic level and restored synaptic transmission and plasticity in hippocampal DG networks lacking miR-26a-3p. Moreover, this inhibition of PTEN also partially alleviated the depression-like behaviors in these CUMS rats. Collectively, these results suggest that the PTEN-PI3K/Akt signaling pathway may act as a downstream component of miR-26a-3p in depression, while the inhibition of this pathway, as accomplished with the PTEN inhibitor, BPV (pic), exerts a neuroprotective effect in depressed rats. It should be point out that the present study mainly investigated

the neuroprotective effects of the PTEN inhibitor BPV (pic) in the central nervous system. However, PTEN also exerts multiple functions in many diseases besides the nervous system via complicated molecular mechanisms. For example, PTEN act as a tumor suppressor involved in breast cancer (54), glioma (55) and leukemia therapy (56). Therefore, it should be taken into consideration the potential side effects or off target effects in the animals using this peripheral administration of BPV (pic). Therefore, the potential effects of the PTEN inhibition on depression would be achieved further investigation in the future studies.

In conclusion, the findings of this report lead to the novel hypothesis that miR-26a-3p, via suppression of the PTEN/PI3K/Akt pathway, plays an important role in the alleviation of neuronal anomalies coupled with depression as induced by CUMS. Accordingly, these results have important biological and clinical significance with regards to the potential identification and treatment of depression disorders.

Methods

Contact for Reagent and Resource Sharing

Further information and requests for resources and reagents should be directed to and will be fulfilled by the Lead Contact, Shu Yan Yu Professor (shuyanyu@sdu.edu.cn).

Animals and housing conditions.

Male Wistar rats (180-200g body weight) were obtained from the Shandong University Animal Centre. All experimental procedures were approved by the Shandong University Animal Care and Use Committee and conform to the National Institutes of Health Guide for the Care and Use of Laboratory Animals (National Research Council, 1996). All efforts were made to minimize the number and suffering of the animals used in the experiments. Rats were housed under standard laboratory conditions for at least one week prior to experimental procedures.

CUMS model.

The rat model of depression consisted of the CUMS procedure as described previously with minor modifications (57). Briefly, rats were housed individually and subjected to chronic stressors including clipping tails (1 min), physical restraint (2h), 5 min cold swimming (4°C), overnight illumination, cage shaking (2h), 24 h food and water deprivation, foot-shock (0.5 mA, 0.5 s) and wet bedding (24h). One stressor was applied daily to each rat in a random order over a 5-week period.

Behavioral tests.

Behavioral tests were used to assess depression-like behaviors in rats after the 5 weeks of

CUMS exposure.

Sucrose preference test (SPT) The sucrose preference test was conducted as described previously (57). In the adaptation phase, rats were permitted accessed to two bottles each containing 1% sucrose solution for 24 h, then one bottle was replaced with tap water for the following 24 h period. In the test phase, after 24 h of food and water deprivation, rats permitted free access to two bottles for 3 h, one containing 100 ml of sucrose solution (1%, w/v) and the other 100 ml of tap water. Sucrose preference was presented as sucrose consumption/ [water consumption + sucrose consumption] ×100%.

Forced swim test (FST) The forced swim test was conducted according to procedures described in previous studies (58, 59). On the training day, rats were placed individually in a water-containing cylinder (height: 80 cm, diameter: 30 cm, temperature: 25 °C) for a 15-min of forced swimming. After 24 h, each rat was placed in the cylinder for a 5-min test period. Durations of immobility (floating except for movements required to maintaining the head above water) and swimming were recorded by an experimenter blind as to the treatment group.

miRNA library construction and sequencing.

Total RNAs isolated from hippocampal DG tissue obtained from control and CUMS group was used for miRNA library preparation and sequencing, as well as used for the

subsequently q-PCR verification. Briefly, total RNA samples were fractionated on a 15% Tris-borate-EDTA (TBE) polyacrylamide gel (Invitrogen) and small RNAs ranging between 18 and 30 nucleotides (nt) were purified and used for library preparation. Small RNAs were reverse transcribed into cRNA and amplified by PCR. The PCR products were sequenced using the Illumina HiSeq^{TM} 2500 platform. The follow-up qPCR analyses were performed to validate the expression levels of some miRNAs from the microarray analysis. The miRNA pathway predication was performed based on DIANA-miRPath (30). The Database for Annotation, Visualization and Integrated Discovery (DAVID) functional annotation was performed for target genes (31). MiRNA target genes implicated in the pathway were investigated among genes with use of the KEGG database (32). A $P < 0.05$ was used as the criterion for statistical significance. The miRNA library preparation and sequencing were performed by Ribo Bio-tech, Guangzhou, China.

Dual-luciferase reporter assay.

Potential targets of miR-26a-3p and PTEN were predicted by TargetScan (www.targetscan.org) and miRDB (www.mirdb.org). For the in vitro luciferase assay, 100 ng of luciferase reporter plasmid (pmirGLO-PTEN or pmirGLO-PTEN-MUT recombinant vector) was co-transfected with 400 ng of miR-26a-3p mimic (over-expression sequence of miR-26a-3p) or miR-NC into cultured human embryonic kidney (HEK)-293T cells

using Lipofectamine 2000 (Invitrogen, 11668027). At 24 h post-transfection, luciferase activities were detected in 293T cells with use of the Dual-Luciferase Reporter Assay System (Promega, Madison, WI, USA) (60)(63).

Stereotaxic injection of the AAV virus.

The AAV9-CMV-eGFP-miR-26a-3p virus (AAV-miR-26a-3p) was constructed to overexpress miR-26a-3p. The primer sequence used for express gene fragments of miR-26a-3p is: ACGAGCTGTACAAGGCTAGCTAACCCCTTCTCTTTGACAGTAG (Gene Chem. Co., Shanghai, China). A sponge sequence form of miR-26a-3p was expressed in the AAV to construct the AAV9-CMV-eGFP-Sponge(miR-26a-3p)-WPRE virus (AAV-miR-26a-3p-sponge), which act as the sponge attached to and inhibit the functions of endogenous miR-26a-3p. The inverse complementary sequence of mature miR-26a-3p is: GTGCAAGTAACCAAGAATAGG (Gene Chem. Co., Shanghai, China). For viral injection, rats were anesthetized with sodium pentobarbital (150 mg/kg, i.p.) and placed in a stereotaxic frame (Stoelting, USA). The skin between the two ears of rats was shaved with a trimming machine and then sanitized with betadine. We used scalpel to make an anterior-posterior incision of about 1.5 cm between the ears. The surface of the skull was cleaned with a cotton swab until the bregma which located at the intersection between the coronal suture and sagittal sutures is visible. Using the tip of the microliter syringe to point

to the bregma point, the coordinates of these three axes were considered as the zero point. According to coordinates of the hippocampal regions in Rat Brain Atlas, viral injection site was focused on the center of hippocampus according to the following coordinates relative to the bregma in mm: -3.24 at the anterior/posterior axis, ±0.5 at the lateral/medial axis and -4.8 at the dorsal/ventral axis. The shallow holes were drilled only in the skull bone with a fine driller. The microliter syringe was placed above the hole and let down slowly vertically until it reached the target hippocampal regions. Purified AAV virus (~ 10^{12} infection units per ml, 1-1.5 ul) were infused bilaterally into hippocampal regions at a rate of 150 nl/min. The microliter syringe remained in the injection site for at least 5 min after infusion and was then slowly withdrawn. Infection efficiency assays were performed at a minimum of 14 days after viral injection. Injection sites were verified and only data from rats with correct injection sites were included in the analyses.

Experimental design.

Rats were randomly assigned to one of the following groups: (1) wide type controls (WT, non-stressed and non-injected group), (2) wide type + AAV-control (WT/eGFP construct), (3) wide type + AAV-miR-26a-3p-sponge, (4) CUMS (5-weeks chronic stress), (5) CUMS + AAV-control (CUMS/eGFP construct), (6) CUMS+AAV-miR-26a-3p, (7) BPV (pic) + WT/AAV-miR-26a-3p-sponge and (8) DMSO + WT/AAV-miR-26a-3p-sponge. For BPV

(pic) (catalog AG-CR1-0043-M005, Adipogen, San Diego, USA) treatment, rats were given BPV (pic) (0.2mg/kg, intra-peritonelly, i.p.) four times at an interval of 3 h as previously described (61), and AAV-miR-26a-3p-sponge was injected 30 min after the last injection. BPV (pic) was dissolved in dimethyl sulfoxide (DMSO, Sigma, St. Louis, MO, USA) and the concentration of DMSO did not exceed 0.1% of the total volume.

Hippocampal Slice Preparations and Whole-Cell Recordings.

Rats were anesthetized using pentobarbital and rapidly decapitated. Hippocampal coronal slices (300 mm in thickness) were sectioned with use of a vibratome (VT-1200s, Leica, Germany) in oxygenated (95% O2/5% CO2), ice-cold cutting solution (pH 7.4) containing (in mM) 30 Glucose, 2.5 KCl, 26 NaHCO3, 7 MgSO4, 1 NaH2PO4, 1 CaCl2, 119 choline chloride, 1 kynurenic acid, 3 sodium pyruvate and 1.3 sodium L-ascorbate. Slices were quickly transferred to the recovery solution containing (in mM) 85 NaCl, 2.5 KCl, 1.25 NaH2PO4, 0.5 CaCl2, 4 MgCl2, 24 NaHCO3, 25 glucose and 50 sucrose. The slices were allowed to recover for 30 min at 36◦C and then a minimum of 1 h at room temperature before recording. Whole-cell patch-clamp recordings in voltage-clamp mode were performed on neurons within the DG hippocampus. In the process of voltage clamp recordings, patch pipettes (3–5 MΩ) were filled with a solution (pH 7.3) containing (in mM): 125 CsCl2, 5 NaCl, 4 Hepes, 0.2 EGTA, 0.2 NaGTP, 2 MgATP, 7 phosphocreatine,

and 2 MgCl2. Excitatory post-synaptic currents (EPSCs) were detected at a holding potential of -70 mV with 50 mM AP-5 and 50 mM picrotoxin present in the artificial cerebrospinal fluid (ACSF) used for perfusion. Miniature excitatory post-synaptic currents (mEPSCs) were recorded with the application of 1 mM TTX in external solutions. During recordings, slices were continuously perfused with ACSF at a rate of ~2 ml/min and at 32 ± 1◦C. sEPSCs and mEPSCs were analyzed using the Mini Analysis Program. Event counts were performed by experimenter blind to the group identity. All recording data were filtered at 2 kHz and digitized at 10 kHz. Data were acquired using digidata 1440A and pCLAMP 10.6 software. Only neurons with sufficiently negative resting membrane potentials (≤ -65 mV) and an absence of spontaneous firing were included in the analysis.

Immunofluorescence assay.

One day after behavioral tests, rats were anesthetized and perfused with 4% paraformaldehyde (PFA). Brains were post-fixed in PFA overnight at 4°C followed by a graded dehydration and then cut into serial coronal frozen slices (30 μm). Slices were incubated with the primary antibodies consisting of anti-synaptophysin (Syn) (1:50, catalog 9020), anti- MAP-2 (1:100, catalog 4542), anti-cleaved caspase-3 (1:100, catalog 9661), anti-DCX (1:200, catalog 4604) (Cell Signaling Technologies), anti-PSD-95 (1:100, catalog 20665-1-AP, Proteintech Group) and anti-Nestin (1:50, catalog PA5-47378,

Thermofish) followed by the fluorescent-conjugated secondary antibody (1:200, catalog SA00013-1, Proteintech Group). Slices were washed in PBS and counterstained with 4′, 6-diamidino-2-phenylindole dihydrochloride (DAPI) (catalog C0060, Solarbio) for 7 min. Images were captured with use of a laser scanning confocal microscope (LSM780, Carl Zeiss, Germany). At least four to six images were taken from each rat for analysis by Image-Pro plus 6.0 software. For the mean intensity of immunofluorescence, the software was used to circle out the hippocampus DG area to measure the area size and the total intensity of immunofluorescence on the area, so as to obtain the mean intensity of immunofluorescence. For the positive cells in DG per mm^2, the software was used to circle out the hippocampus DG area to measure the size of the area and the total number of positive cells, so as to obtain the number of positive cells per mm^2.

Golgi Staining.

Golgi staining was performed to examine changes in neuronal dendritic spines using the FD Rapid GolgiStain™ Kit (PK401, FD Neuro-Technologies, MD21041, USA) according to the manufacturers' instructions. Briefly, rats were anaesthetized and brains rapidly removed and immersed in the impregnation solution (A/B=1:1, total 15 ml/rat) for two weeks. Brain samples were cut into 100 μm coronal slides and cleaned in xylene. Slides were then cover-slipped with Rhamsan gum for light microscopic observation. Apical

dendrites of neurons were chosen for morphological analysis. For each group, at least 4 to 6 dendritic segments per neuron were randomly selected and at least 5 pyramidal neurons were analyzed per rat. The number of spines was analyzed with use of Image-Pro plus software.

Electron microscopy analysis.

Transmission electron microscopy (TEM) was used to examine synapses and ultrastructures of neurons. DG tissue samples (1×1×1mm) were carefully dissected and placed in 2.5% glutaraldehyde at 4°C for 2-4 h. The tissue was fixed with 1% OsO4 in 0.1 M PBS (pH 7.4) for 1 h and subjected to a graded ethanol dehydration, followed by infiltration with a mixture of one-half propylene oxide overnight. Tissues were embedded in resin, cut into ultrathin sections (70 nm thick) and stained with 4% uranyl acetate for 20 min followed by staining with 0.5% lead citrate for 15 min. Sections were examined under a TEM (Philips Tecnai 20 U-Twin, Holland). At least 20 micrographs were randomly selected from each rat for analysis using Image J software (NIH, Scion Corporation, Frederick, MD).

Reverse transcription PCR and quantitative real-time PCR.

Total RNA from DG regions was isolated using the RNA rapid extraction kit（Aidlab，

China) according to the manufacturers' instructions. Total RNA was reverse transcribed into cDNA and subsequently amplified by PCR with specific primers (Supplementary Table 1). PCR products were separated by electrophoresis and images were obtained using the Gel Image Analysis System (Bio-rad, USA). Intensities of bands were analyzed using Image-Pro Plus 6.0 software and values were normalized to GAPDH.

Quantitative real time-PCR was performed with use of the Bio-rad IQ5 Real Time PCR System (Bio-Rad, USA). The relative fold change in expression of miRNA was determined using the the 2^{-} ($\Delta\Delta$Ct) method. GAPDH served as a loading control in each group.

Western blot analysis.

DG regions were carefully isolated and immediately homogenized in lysis buffer with a cocktail of protease inhibitors. Protein concentrations were determined using the BCA assay kit (Beyotime, China). Proteins (30 ug) from each sample were electrophoretically separated on 8–15% gradients of SDS-PAGE gels, transferred to PVDF membranes and probed with the following primary antibodies, anti-BDNF (1:300, catalog sc-546, Santa Cruz Biotechnology Inc.), anti-CREB (1:500, catalog 9197), anti-PSD95 (1:1000, catalog 3450); anti-synaptophysin (1:1000, catalog 5461), anti- LC3I/II (1:1000, catalog 12741), anti-Beclin1 (1:1000, catalog 3495), anti- PARP (1:1000, catalog 9532), anti-cleaved

caspase3 (1:500, catalog 9661), anti-PTEN (1:500, catalog 9552), anti-PI3K (1:500, catalog 4292), anti-p-Akt (1:500, catalog 9271), anti-p53 (1:500, catalog 9284), anti-p62 (1:1000, catalog 23214), anti-β-actin (1:1000, catalog 4970) (Cell Signaling Technologies), anti-caspase9 (1:500, catalog AP0359, Bioworld), anti-BAX (1:1000, catalog 50599-2-lg) and anti-GAPDH (1:4000, catalog 10494-1-AP) (Proteintech Group). The secondary antibody was horseradish peroxidase-conjugated to mouse anti-rabbit/mouse Ig G (1:5000, catalog 16473-1-AP, Proteintech Group). Protein band densities were quantified using Image-J software (NIH, Scion Corporation, Frederick, MD). The samples of each rat was replicated at least three times and final data were expressed as a percent of the control group.

Statistics.

All statistical procedures were performed using GraphPad prism 5. All data were presented as the means ± standard error of the mean (S.E.M.). Pearson's Coefficient tests were performed to analyze statistical significance in expression levels of miRNAs between normal controls and CUMS samples in the small RNA sequencing analysis. The remaining data were analyzed with use of one- or two-way analysis of variance (ANOVA) followed by the Tukey's test for multiple post-hoc comparisons of means. Student t-tests were employed for comparisons between two groups if appropriate. A $P < 0.05$ was required for

results to be considered as statistically significant.

Study approval. The animal studies presented here were approved by the Animal Care and Use Committee of the University of Shandong University (ECSBMSSDU-2018-2-056).

Author Contributions

S.Y.Y. conceived of and designed the research study. Y.L. acquired and analyzed data. Y.L., C.F., L. W., T.L., R.G. and W.W. performed the experiments. S.Y.Y. wrote the paper.

Acknowledgments

This study was supported by grants to Shu Yan Yu from the National Natural Science Foundation of China (NSFC81873796, 82071513), the Natural Science Foundation of Shandong Province of China (ZR2020ZD25) and the Fundamental Research Funds of Shandong University (2018JC008). We thank the staff of the electronic microscope laboratory of experimental center in the basic medical school for technical assistance.

Declaration of Interests

The authors have declared that no conflict of interest exists.

Materials & Correspondence.

Correspondence and material requests should be addressed to S.Y.Y.

Reference

1. Oh DH, et al. Neuropathological abnormalities of astrocytes, GABAergic neurons, and pyramidal neurons in the dorsolateral prefrontal cortices of patients with major depressive disorder. Eur Neuropsychopharmacol. 2012;22(5):330-338.

2. Stockmeier CA, et al. Cellular changes in the postmortem hippocampus in major depression. Biol Psychiatry. 2004;56(9):640-650.

3. Boldrini M, et al. Hippocampal Granule Neuron Number and Dentate Gyrus Volume in Antidepressant-Treated and Untreated Major Depression. Neuropsychopharmacology. 2013;38(6):1068-1077.

4. Krishnan V, and Nestler EJ. The molecular neurobiology of depression. Nature. 2008;455(7215):894-902.

5. Bastos AG, et al. The efficacy of long-term psychodynamic psychotherapy, fluoxetine and their combination in the outpatient treatment of depression. Psychotherapy Research. 2015;25(5):612-624.

6. Gaynes BN, et al. What Did STAR*D Teach Us? Results From a Large-Scale, Practical, Clinical Trial for Patients With Depression. Psychiatr Serv. 2009;60(11):1439-1445.

7. Adzic M, et al. Therapeutic Strategies for Treatment of Inflammation-related Depression. Curr Neuropharmacol. 2018;16(2):176-209.

8. Wong CH, et al. Estimation of clinical trial success rates and related parameters (vol 20, pg 273, 2019). Biostatistics. 2019;20(2):366-366.

9. Savitz J, and Drevets WC. Bipolar and major depressive disorder: Neuroimaging the develop mental-degenerative divide. Neurosci Biobehav Rev. 2009;33(5):699-771.

10. Goldwater DS, et al. Structural and functional alterations to rat medial prefrontal cortex following chronic restraint stress and recovery. Neuroscience. 2009;164(2):798-808.

11. Fernandes J, and Gupta GL. N-acetylcysteine attenuates neuroinflammation associated depressive behavior induced by chronic unpredictable mild stress in rat. Behav Brain Res. 2019;364:356-365.

12. Park SC. Neurogenesis and antidepressant action. Cell Tissue Res. 2019;377(1):95-106.

13. Kubera M, et al. In animal models, psychosocial stress-induced (neuro)inflammation, apoptosis and reduced neurogenesis are associated to the onset of depression. Prog Neuropsychopharmacol Biol Psychiatry. 2011;35(3):744-759.

14. Presutti C, et al. Non coding RNA and brain. BMC Neurosci. 2006;7.

15. Pasquinelli AE. NON-CODING RNA MicroRNAs and their targets: recognition, regulation and an emerging reciprocal relationship. Nature Reviews Genetics.

2012;13(4):271-282.

16. Nowak JS, and Michlewski G. miRNAs in development and pathogenesis of the nervous system. Biochem Soc Trans. 2013;41:815-820.

17. Marangon D, et al. MicroRNAs change the games in central nervous system pharmacology. Biochem Pharmacol. 2019;168:162-172.

18. Su LN, et al. Network analysis of microRNAs, transcription factors, and target genes involved in axon regeneration. Journal of Zhejiang University-Science B. 2018;19(4):293-304.

19. McNeill E, and Van Vactor D. MicroRNAs Shape the Neuronal Landscape. Neuron. 2012;75(3):363-379.

20. Cao DD, et al. MicroRNAs: Key Regulators in the Central Nervous System and Their Implication in Neurological Diseases. Int J Mol Sci. 2016;17(6).

21. Lopez JP, et al. MicroRNAs 146a/b-5 and 425-3p and 24-3p are markers of antidepressant response and regulate MAPK/Wnt-system genes. Nature Communications. 2017;8.

22. Gibbons A, et al. Changes in Non-Coding RNA in Depression and Bipolar Disorder: Can They Be Used as Diagnostic or Theranostic Biomarkers? Noncoding RNA. 2020;6(3).

23. Solich J, et al. Restraint Stress in Mice Alters Set of 25 miRNAs Which Regulate Stress- and Depression-Related mRNAs. Int J Mol Sci. 2020;21(24).

24. Malhi GS, and Mann JJ. Depression. Lancet. 2018;392(10161):2299-2312.

25. Willner P, et al. The neurobiology of depression and antidepressant action. Neurosci Biobehav Rev. 2013;37(10):2331-2371.

26. Fan CQ, et al. Curcumin Protects Against Chronic Stress-induced Dysregulation of Neuroplasticity and Depression-like Behaviors via Suppressing IL-1 beta Pathway in Rats. Neuroscience. 2018;392:92-106.

27. Wang P, et al. Interleukin-6: Its role and mechanisms in rescuing depression-like behaviors in rat models of depression. Brain Behavior and Immunity. 2019;82:106-121.

28. Fan CQ, et al. Neuroprotective Effects of Ginsenoside-Rg1 Against Depression-Like Behaviors via Suppressing Glial Activation, Synaptic Deficits, and Neuronal Apoptosis in Rats. Front Immunol. 2018;9.

29. Miao C, and Chang J. The important roles of microRNAs in depression: new research progress and future prospects. J Mol Med (Berl). 2021.

30. Vlachos IS, et al. DIANA miRPath v.2.0: investigating the combinatorial effect of microRNAs in pathways. Nucleic Acids Res. 2012;40(W1):W498-W504.

31. Huang DW, et al. Systematic and integrative analysis of large gene lists using DAVID bioinformatics resources. Nat Protoc. 2009;4(1):44-57.

32. Kanehisa M, et al. From genomics to chemical genomics: new developments in KEGG. Nucleic Acids Res. 2006;34:D354-D357.

33. Xie L, et al. MicroRNA-26a-2 maintains stress resiliency and antidepressant efficacy by targeting the serotonergic autoreceptor HTR1A. Biochem Biophys Res Commun. 2019;511(2):440-446.

34. Huse JT, et al. The PTEN-regulating microRNA miR-26a is amplified in high-grade glioma and facilitates gliomagenesis in vivo. Genes Dev. 2009;23(11):1327-1337.

35. Mavrakis KJ, et al. A cooperative microRNA-tumor suppressor gene network in acute T-cell lymphoblastic leukemia (T-ALL). Nat Genet. 2011;43(7):673-678.

36. Liu B, et al. MiR-26a enhances metastasis potential of lung cancer cells via AKT pathway by targeting PTEN. Biochim Biophys Acta. 2012;1822(11):1692-1704.

37. van Dijk MT, et al. Altered Dentate Gyrus Microstructure in Individuals at High Familial Risk for Depression Predicts Future Symptoms. Biological Psychiatry-Cognitive Neuroscience and Neuroimaging. 2021;6(1):50-58.

38. Santos MAO, et al. Global hippocampal atrophy in major depressive disorder: a meta-analysis of magnetic resonance imaging studies. Trends Psychiatry Psychother. 2018;40(4):369-378.

39. Roman-Albasini L, et al. Antidepressant-relevant behavioral and synaptic molecular effects of long-term fasudil treatment in chronically stressed male rats. Neurobiol Stress. 2020;13:100234.

40. Schratt GM, et al. A brain-specific microRNA regulates dendritic spine development

(vol 439, pg 283, 2006). Nature. 2006;441(7095):902-902.

41. Jiang JJ, et al. MicroRNA-26a supports mammalian axon regeneration in vivo by suppressing GSK3 beta expression. Cell Death Dis. 2015;6.

42. Lucci C, et al. Spatiotemporal regulation of GSK3 beta levels by miRNA-26a controls axon development in cortical neurons. Development. 2020;147(3).

43. Li F, et al. miR-26a prevents neural stem cells from apoptosis via beta-catenin signaling pathway in cardiac arrest-induced brain damage. Biosci Rep. 2019;39.

44. Lafourcade CA, et al. A Role for mir-26a in Stress: A Potential sEV Biomarker and Modulator of Excitatory Neurotransmission. Cells. 2020;9(6).

45. Lai JP, et al. Phosphatase and tensin homologue deleted on chromosome ten (PTEN) as a molecular target in lung epithelial wound repair. Br J Pharmacol. 2007;152(8):1172-1184.

46. Wang X, et al. Resveratrol protects the integrity of alveolar epithelial barrier via SIRT1/PTEN/p-Akt pathway in methamphetamine-induced chronic lung injury. Cell Prolif. 2020;53(3).

47. Qin Y, et al. mir-106a regulates cell proliferation and apoptosis of colon cancer cells through targeting the PTEN/PI3K/AKT signaling pathway. Oncol Lett. 2018;15(3):3197-3201.

48. Huang EJ, and Reichardt LF. Neurotrophins: Roles in neuronal development and

function. Annu Rev Neurosci. 2001;24:677-736.

49. Leal G, et al. BDNF-induced local protein synthesis and synaptic plasticity. Neuropharmacology. 2014;76:639-656.

50. Baehrecke EH. Autophagy: Dual roles in life and death? Nature Reviews Molecular Cell Biology. 2005;6(6):505-510.

51. Ding J, et al. Inhibition of Phosphatase and Tensin Homolog Deleted on Chromosome 10 Decreases Rat Cortical Neuron Injury and Blood-Brain Barrier Permeability, and Improves Neurological Functional Recovery in Traumatic Brain Injury Model. PLoS One. 2013;8(11).

52. Borges GA, et al. Pharmacological PTEN inhibition: potential clinical applications and effects in tissue regeneration. Regen Med. 2020;15(2):1329-1344.

53. Pulido R. PTEN Inhibition in Human Disease Therapy. Molecules. 2018;23(2).

54. Zhou J, et al. Activation of the PTEN/mTOR/STAT3 pathway in breast cancer stem-like cells is required for viability and maintenance. Proc Natl Acad Sci U S A. 2007;104(41):16158-16163.

55. Dasari VR, et al. Upregulation of PTEN in glioma cells by cord blood mesenchymal stem cells inhibits migration via downregulation of the PI3K/Akt pathway. PLoS One. 2010;5(4):e10350.

56. Martelli AM, et al. Targeting the translational apparatus to improve leukemia therapy:

roles of the PI3K/PTEN/Akt/mTOR pathway. Leukemia. 2011;25(7):1064-1079.

57. Mao QQ, et al. Peony glycosides produce antidepressant-like action in mice exposed to chronic unpredictable mild stress: Effects on hypothalamic-pituitary-adrenal function and brain-derived neurotrophic factor. Prog Neuropsychopharmacol Biol Psychiatry. 2009;33(7):1211-1216.

58. Porsolt RD, et al. Depression: a new animal model sensitive to antidepressant treatments. Nature. 1977;266(5604):730-732.

59. Duman CH, et al. A role for MAP kinase signaling in behavioral models of depression and antidepressant treatment. Biol Psychiatry. 2007;61(5):661-670.

60. Li Z, et al. MicroRNA-23b Promotes Avian Leukosis Virus Subgroup J (ALV-J) Replication by Targeting IRF1. Sci Rep. 2015;5:10294.

61. Zhang QG, et al. Critical role of PTEN in the coupling between PI3K/Akt and JNK1/2 signaling in ischemic brain injury. FEBS Lett. 2007;581(3):495-505.

Figures

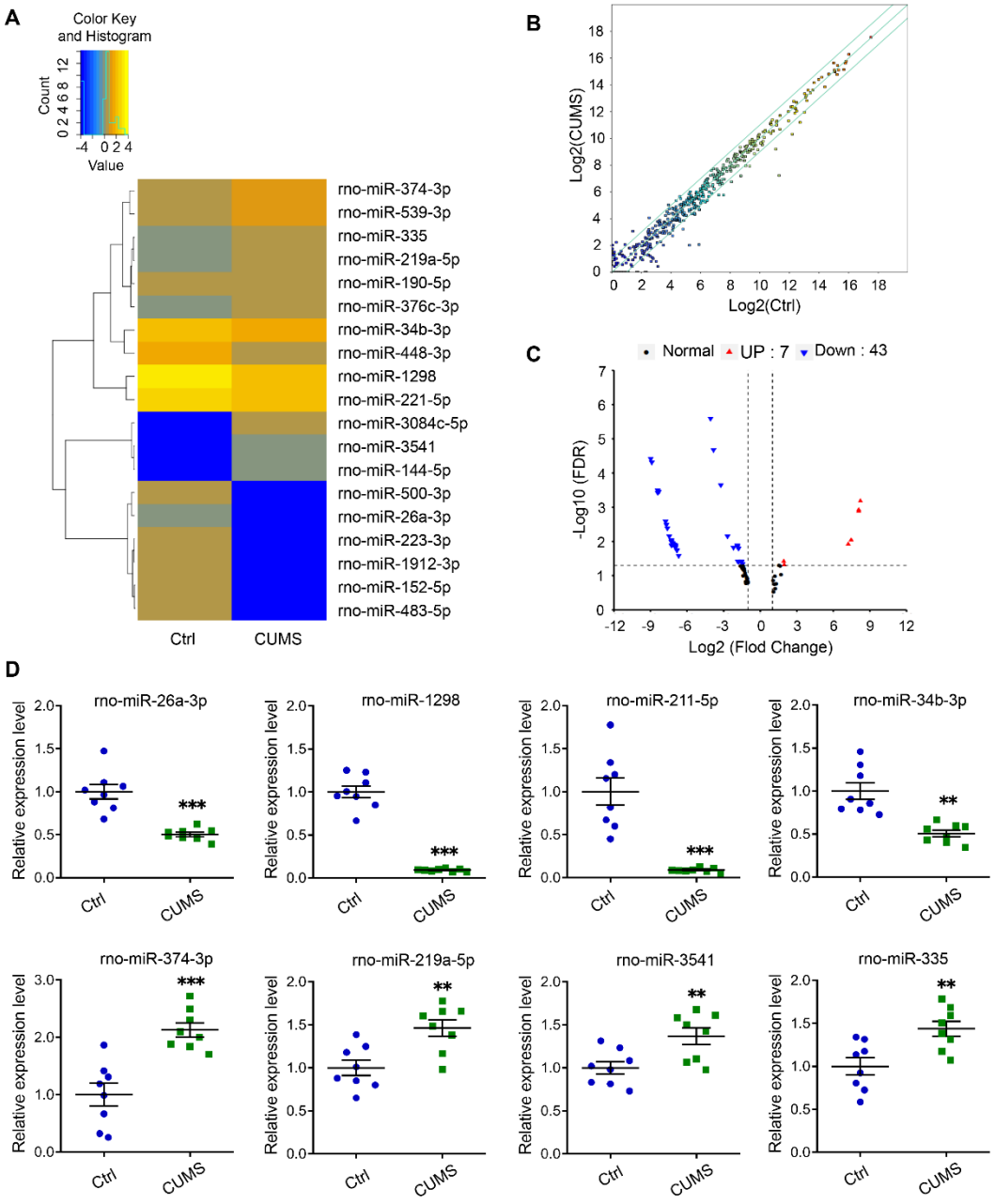

Figure. 1. MiRNA expression profiles of DG tissue derived from control and CUMS-induced depression groups. (**A)** Representative heatmap diagram of differential miRNA

expression levels by sequencing on the Illumina HiSeq 2500 platform. N = 3 rats per group. (**B)** Scatter plots were used to evaluate differences in the expression of miRNAs between the two groups. The miRNAs above the top green line and below the bottom green line indicate a > 2.0 fold change between the two groups. N = 3 rats per group. (**C)** Volcano plots indicated differential expressions between the two groups. A $P < 0.05$ and fold change > 2 were considered as statistically significant. N = 3 rats per group. (**D)** The expression levels of eight miRNAs were validated by qPCR in DG tissues. N = 8 rats per group. Experiments performed in triplicate with 3 biological replicates for all panels. Data represent means ± SEM. $^{**}P < 0.01$, $^{***}P < 0.001$ vs. control by Student's t test. Ctrl, control.

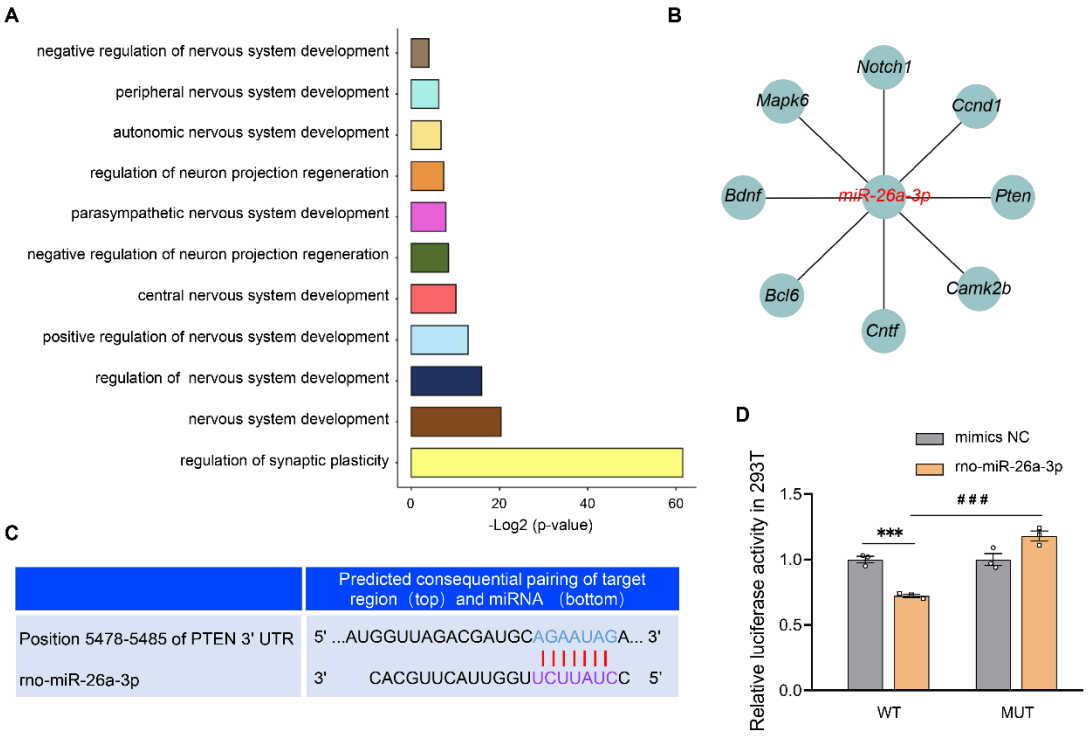

Figure. 2. Prediction and validation of target genes of miR-26a-3p and its signaling pathways. (**A)** DAVID function annotation for the miR-26a-3p targeted genes with horizontal axes showing −log2 transformed P-values. **(B)** Bioinformatical prediction of eight target genes of miR-26a-3p by DIANA-miRPath appear to be related with pathways in depression. **(C)** Putative seed-matching sites between miR-26a-3p and PTEN. **(D)** Dual-Luciferase reporter assay was performed to detect relative luciferase activities of WT and MUT PTEN reporters. N = 3 per group. Experiments repeated at least 3 times. Data represent means ± SEM. ***$P < 0.001$ vs. WT + mimics NC; $^{\#\#\#}P < 0.001$ vs. WT + rno-miR-26a-3p by one-way ANOVA with post hoc Tukey's correction. WT, wide type; MUT, mutation.

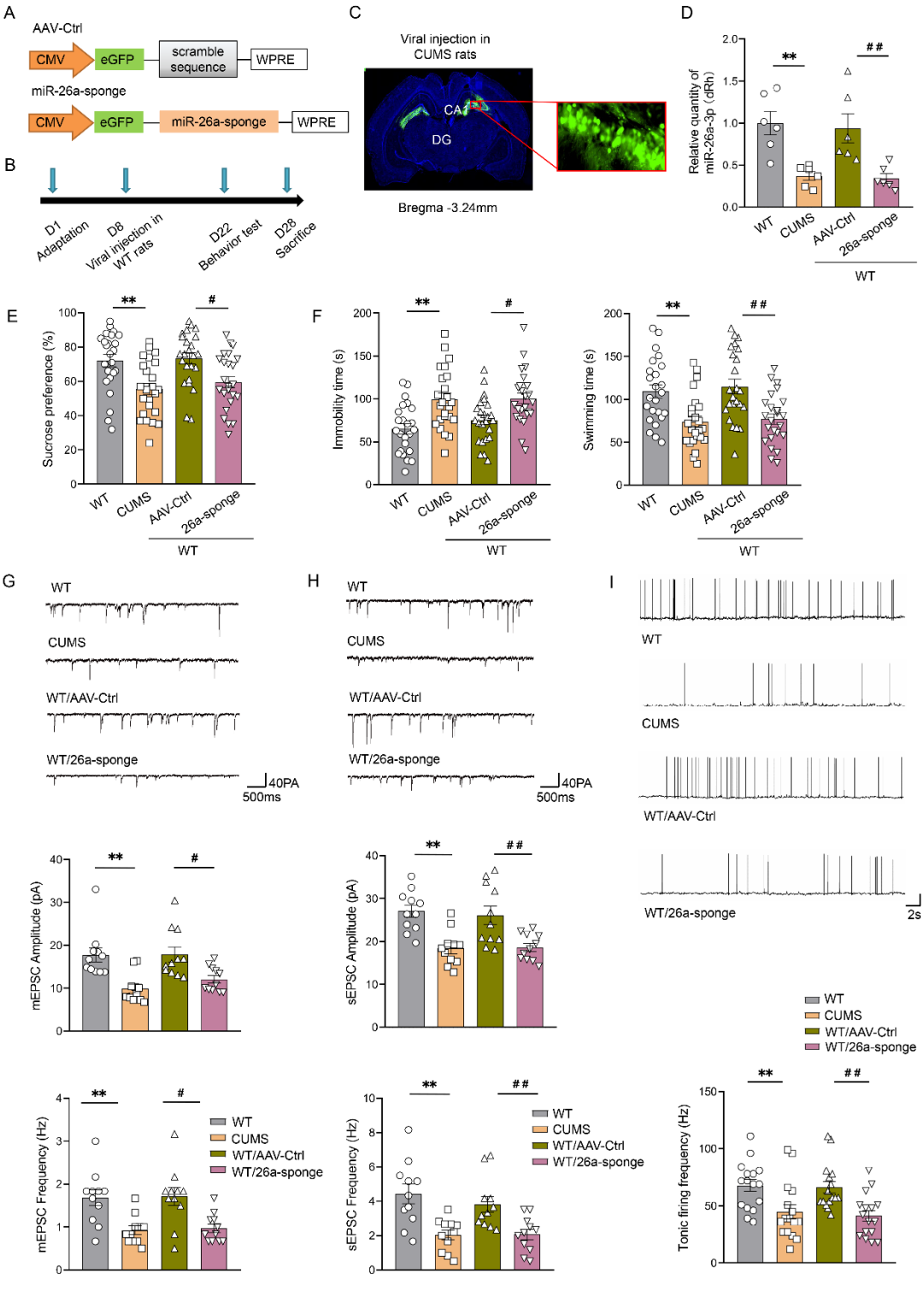
A
AAV-Ctrl
CMV
eGFP
scramble sequence
WPRE
miR-26a-sponge
CMV
eGFP
miR-26a-sponge
WPRE
B
D1 Adaptation
D8 Viral injection in WT rats
D22 Behavior test
D28 Sacrifice
C
Viral injection in CUMS rats
CA1
DG
Bregma -3.24mm
D
Relative quantity of miR-26a-3p (dRh)
WT
CUMS
AAV-Ctrl
26a-sponge
WT
E
Sucrose preference (%)
F
Immobility time (s)
Swimming time (s)
G
WT
CUMS
WT/AAV-Ctrl
WT/26a-sponge
40PA
500ms
H
WT
CUMS
WT/AAV-Ctrl
WT/26a-sponge
40PA
500ms
I
WT
CUMS
WT/AAV-Ctrl
WT/26a-sponge
20mV
2s
mEPSC Amplitude (pA)
sEPSC Amplitude (pA)
mEPSC Frequency (Hz)
sEPSC Frequency (Hz)
Tonic firing frequency (Hz)
WT
CUMS
WT/AAV-Ctrl
WT/26a-sponge

Figure. 3. Knock-down of miR-26a-3p within the DG induced depression-like behaviors in normal rats. **(A)** Schematics of AAV vectors engineered to knock-down miR-26a-3p or a vector control construct. **(B)** Experimental paradigm for viral injection and behavioral testing. **(C)** Illustration of bilateral viral injection site in the DG hippocampus. Scale bar = 20μm. **(D)** Quantitative real-time PCR was used to validate the efficiency of miR-26a-3p knock-down. N = 6 rats per group. Three independent biological replicate experiments were performed for each group. **(E)** Knock-down of miR-26a-3p within the DG decreased sucrose consumption in the sucrose preference test and **(F)** increased immobility times and decreased swimming times of rats in the forced swim test. N = 18 rats per group for behavioral test. Knock-down of miR-26a-3p in DG neurons produced changes in **(G)** mEPSC, **(H)** sEPSC and (**I**) spontaneous burst activity. N = 10 cells from 6 rats per group in (**G** and **H**). N = 16 cells from 6 rats per group in (**I**). Electrophysiological recording was repeated at least 3 independent experiments. Data are presented as the means ± SEM. $^{**}P < 0.01$ vs. WT; $^{\#}P < 0.05$, $^{\#\#}P < 0.01$ vs. AAV-control (WT+ AAV-control) by ANOVA with post hoc Tukey's correction. WT, wide type; Ctrl, control.

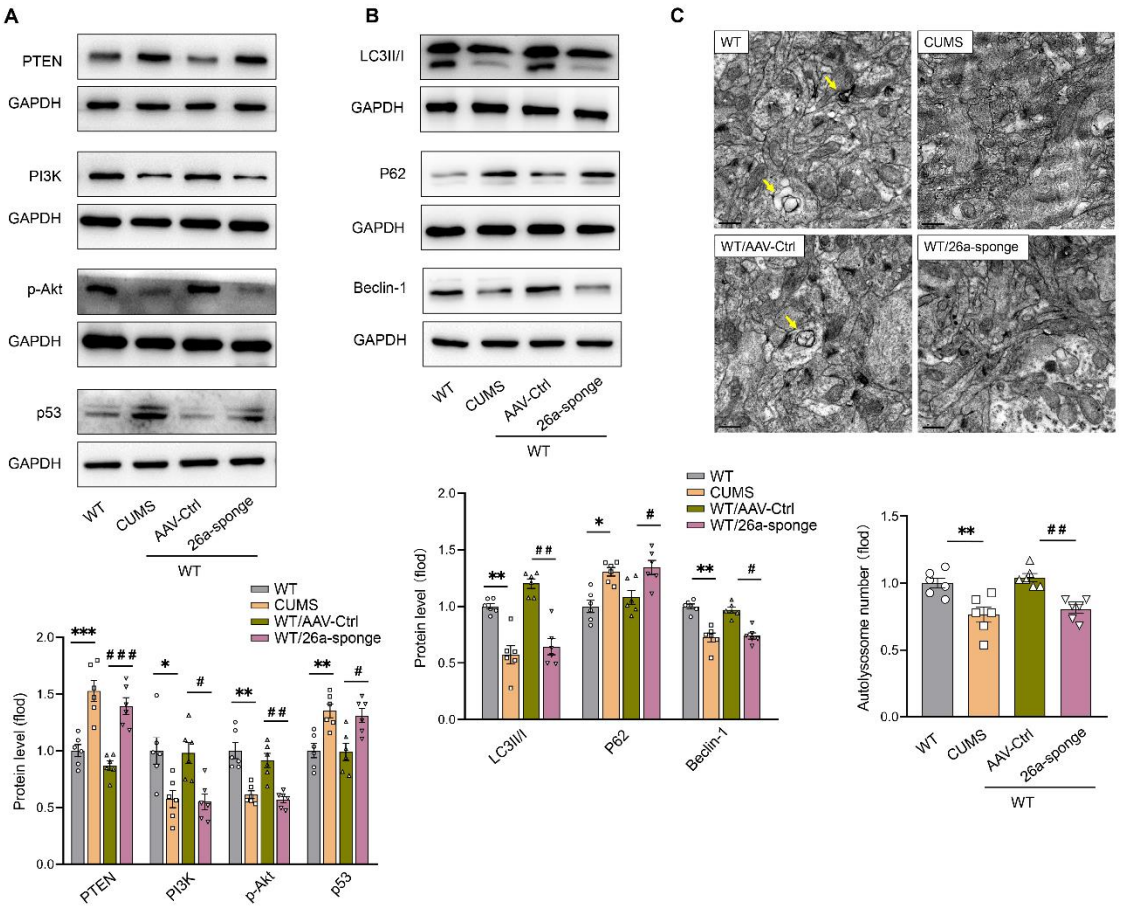

Figure. 4. Knock-down of miR-26a-3p within the DG inhibited autophagy in normal rats. **(A)** Knock-down of miR-26a-3p increased expressions of PTEN and p53, accompanied with decreased expressions of PI3K and phosphorylated Akt within the DG. N = 6 rats per group. **(B)** Knock-down of miR-26a-3p decreased expressions of LC3-II/I ratios and Beclin-1expression, accompanied with increased expressions of p62. N = 6 rats per group. **(C)** Knock-down of miR-26a-3p decreased the number of autolysosomes in the DG. N = 6 rats per group and at least 20 micrographs from 1 animal. Scale bar = 500nm. Experiments performed in triplicate with 3 biological replicates for all panels. Data are presented as the

means ± SEM. *$P < 0.05$, **$P < 0.01$, ***$P < 0.001$ vs. WT; $^{\#}P < 0.05$, $^{\#\#}P < 0.01$, $^{\#\#\#}P < 0.001$ vs. AAV-control (WT+ AAV-control) by ANOVA with Tukey's post hoc correction. WT, wide type; Ctrl, control.

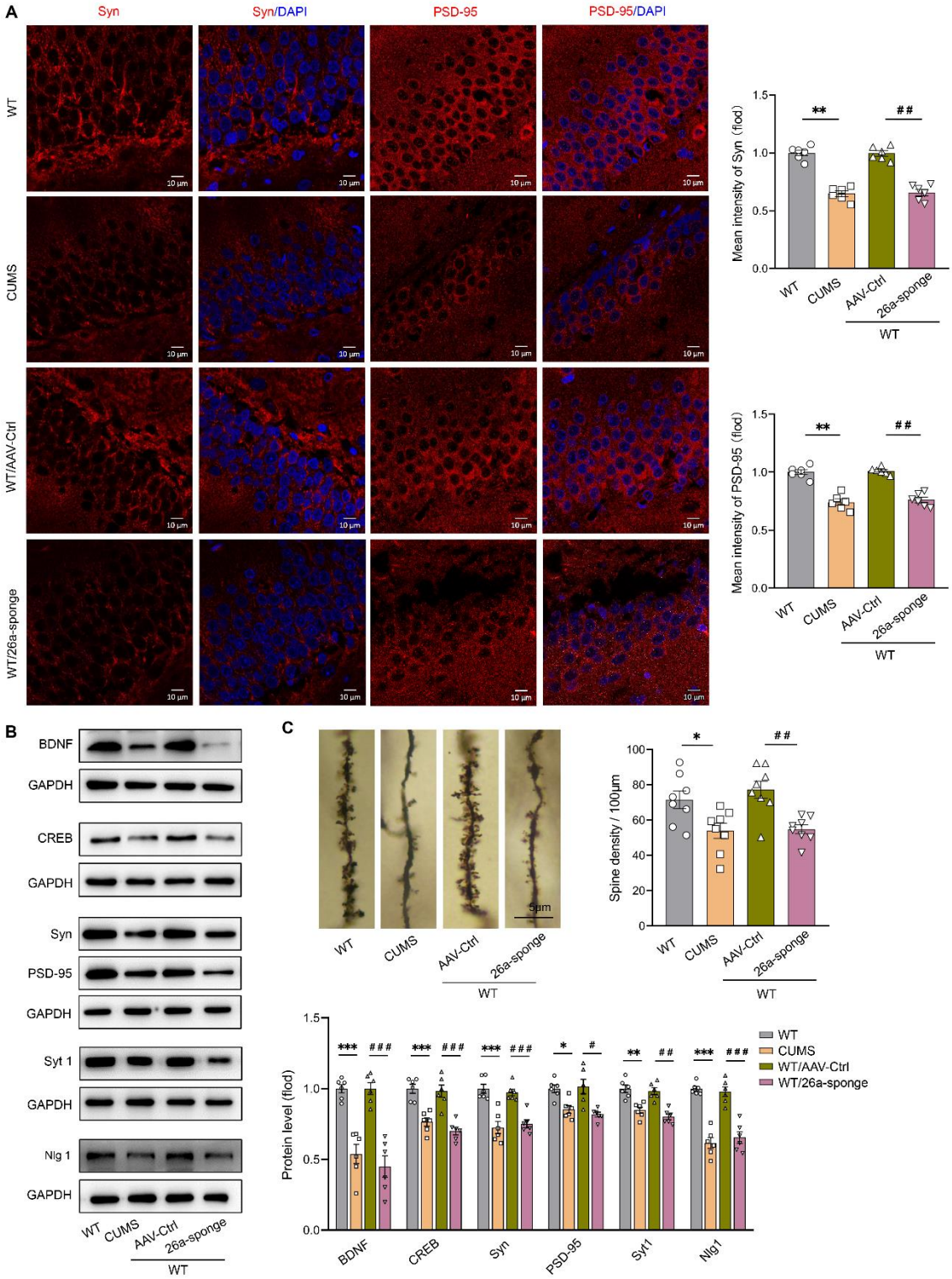
A
Syn
Syn/DAPI
PSD-95
PSD-95/DAPI
WT
CUMS
WT/AAV-Ctrl
WT/26a-sponge
10 μm
Mean intensity of Syn (flod)
Mean intensity of PSD-95 (flod)
WT
CUMS
AAV-Ctrl
26a-sponge
B
BDNF
GAPDH
CREB
Syn
PSD-95
Syt 1
Nlg 1
C
5μm
Spine density / 100μm
Protein level (flod)
BDNF
CREB
Syn
PSD-95
Syt1
Nlg1
WT
CUMS
WT/AAV-Ctrl
WT/26a-sponge

Figure. 5. Knock-down of miR-26a-3p within the DG of normal rats induced dysregulation of neuroplasticity. **(A)** Representative confocal microscopic images showing expressions of Syn and PSD-95within the DG of different groups. Scale bar = 10μm. N=6 rats per group and at least 4-6 images from 1 animal. **(B)** Knock-down of miR-26a-3p decreased protein levels of neuroplasticity-related mediators in the DG. N = 6 rats per group. Blot results of Syn and PSD-95 were from the same samples and run parallelly in different gels. Three independent biological replicate experiments were performed. **(C)** Representative Golgi staining images and summary of data showing dendritic spines in DG neurons of different groups. Scale bar = 5μm. N = 8 rats per group and at least 5 pyramidal neurons from 1 animal. Immunofluorescence and Golgi staining were repeated at least 3 times and quantitation was done for representative samples from each group. Data are presented as the means ± SEM. $^{*}P < 0.05$, $^{**}P < 0.01$, $^{***}P < 0.01$ vs. WT; $^{\#}P < 0.05$, $^{\#\#}P < 0.01$, $^{\#\#\#}P < 0.001$ vs. AAV-control (WT+ AAV-control) by ANOVA with Tukey's post hoc correction. WT, wide type; Ctrl, control.

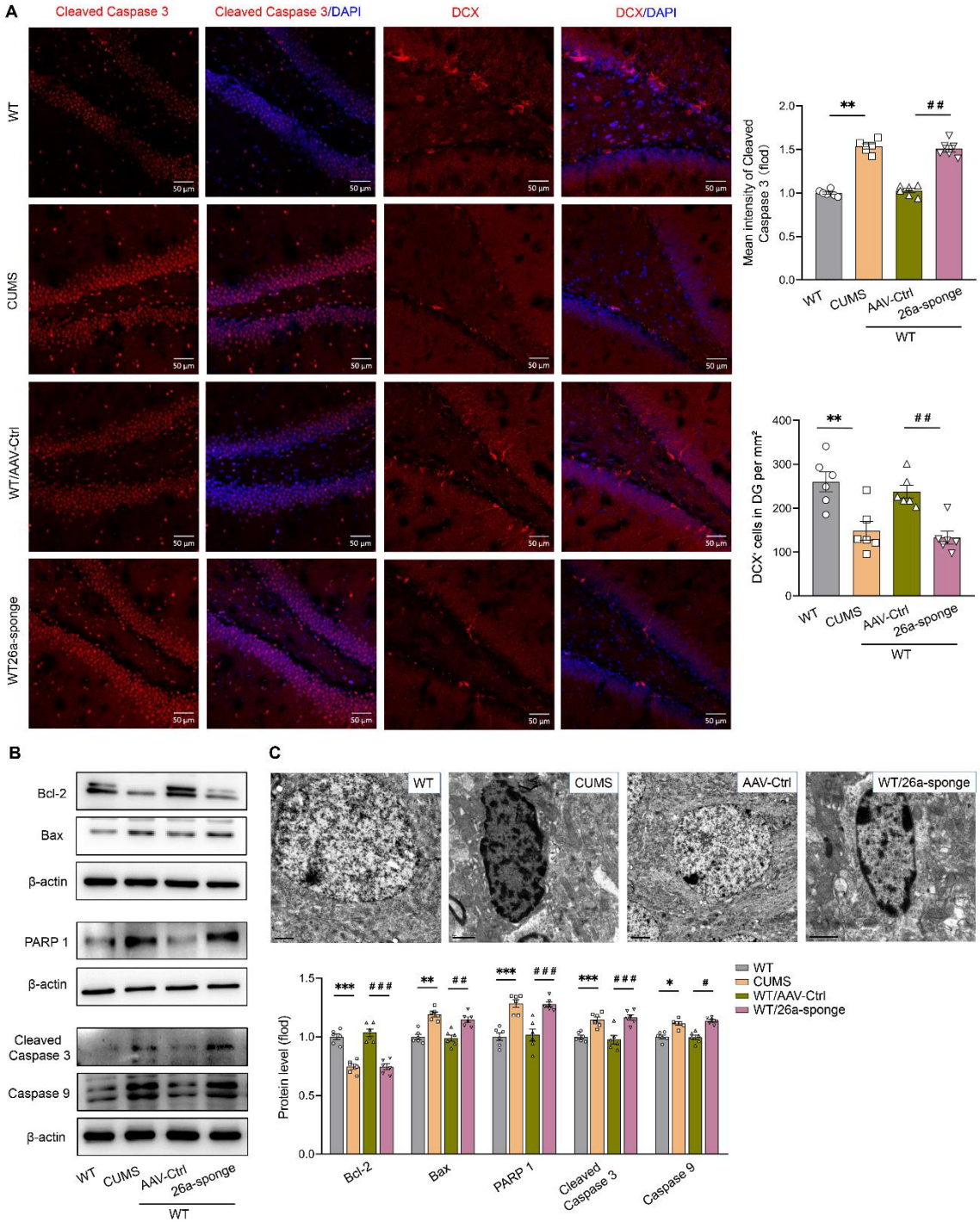

Figure. 6. Knock-down of miR-26a-3p within the DG of normal rats induced neuronal

apoptosis. **(A)** Representative confocal microscopic images showing expressions of cleaved caspase-3 and DCX within the DG of different groups. Scale bar = 50μm. N = 6 rats per group and at least 4-6 images from 1 animal. **(B)** Knock-down of miR-26a-3p increased protein levels of pro-apoptotic factors in the DG. N=6 rats per group. Blot results were from the same samples and run parallelly in different gels. Three independent biological replicate experiments were performed. **(C)** Representative electronic micrographs showing nuclear chromatin abnormalities in DG neurons of different groups. Scale bar = 1 μm. N = 6 per group and at least 5 pyramidal neurons from 1 animal. Immunofluorescence and electron microscope experiments were repeated at least 3 times and quantitation was done for representative samples from each group. Data are presented as the means ± SEM. $*P < 0.05$, $**P < 0.01$, $***P<0.001$ vs. WT; $^{\#}P < 0.05$, $^{\#\#}P < 0.01$, $^{\#\#\#}P < 0.001$ vs. AAV-control (WT+ AAV-control) by ANOVA with Tukey post hoc correction. WT, wide type; Ctrl, control.

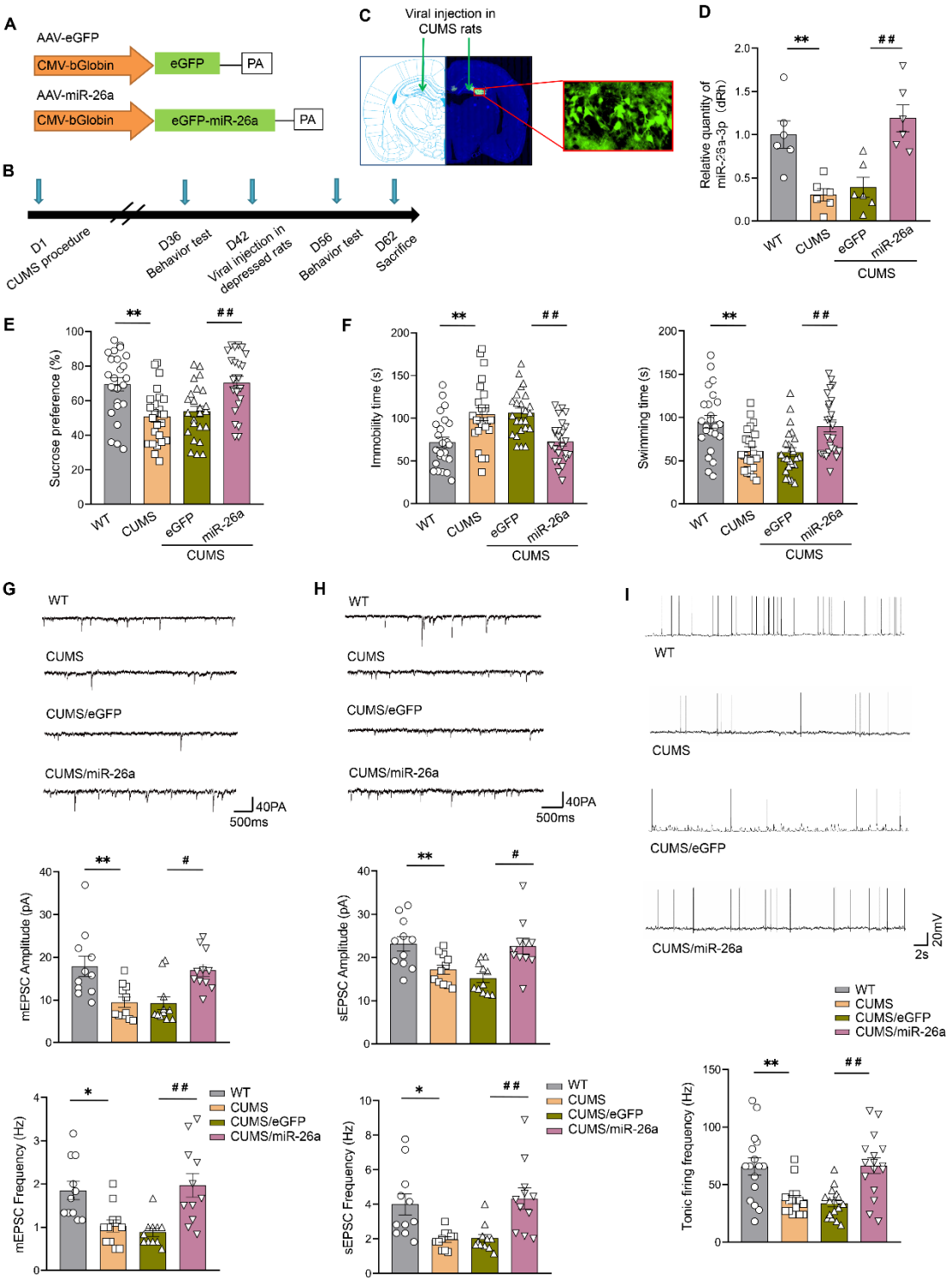

Figure. 7. Overexpression of miR-26a-3p in the DG of CUMS rat rescues depression-like

symptoms produced by CUMS exposure. **(A)** Construct of AAV-miR-26a-3p to overexpress miR-26a-3p. CMV and promoter. **(B)** Experimental paradigm for CUMS, viral injection and behavioral testing. **(C)** Representative site of viral injection in the DG. Scale bar = 20μm. **(D)** Quantitative real-time PCR showing efficiency of miR-26a-3p overexpression in DG regions. N = 6 rats per group. Three independent biological replicate experiments were performed for each group. **(E)** Overexpression of miR-26a-3p in the DG of CUMS rats increased sucrose consumption in the sucrose preference test and **(F)** decreased immobility times and increased swimming times in the forced swim test. N = 18 rats per group for behavioral test. Overexpression of miR-26a-3p in DG neurons produced changes in **(G)** mEPSC **(H)** sEPSC and **(I)** spontaneous burst activity. N = 11 cells from 6 rats per group in (**G** and **H**). N = 16 cells from 6 rats per group in (**I**). Electrophysiological recording was repeated at least 3 independent experiments. Data are presented as the means ± SEM. $*P < 0.05$, $**P < 0.01$ vs. WT; $^{\#}P < 0.05$, $^{\#\#}P < 0.01$ vs. eGFP control (CUMS+ AAV-eGFP) by ANOVA with Tukey post hoc correction. WT, wide type.

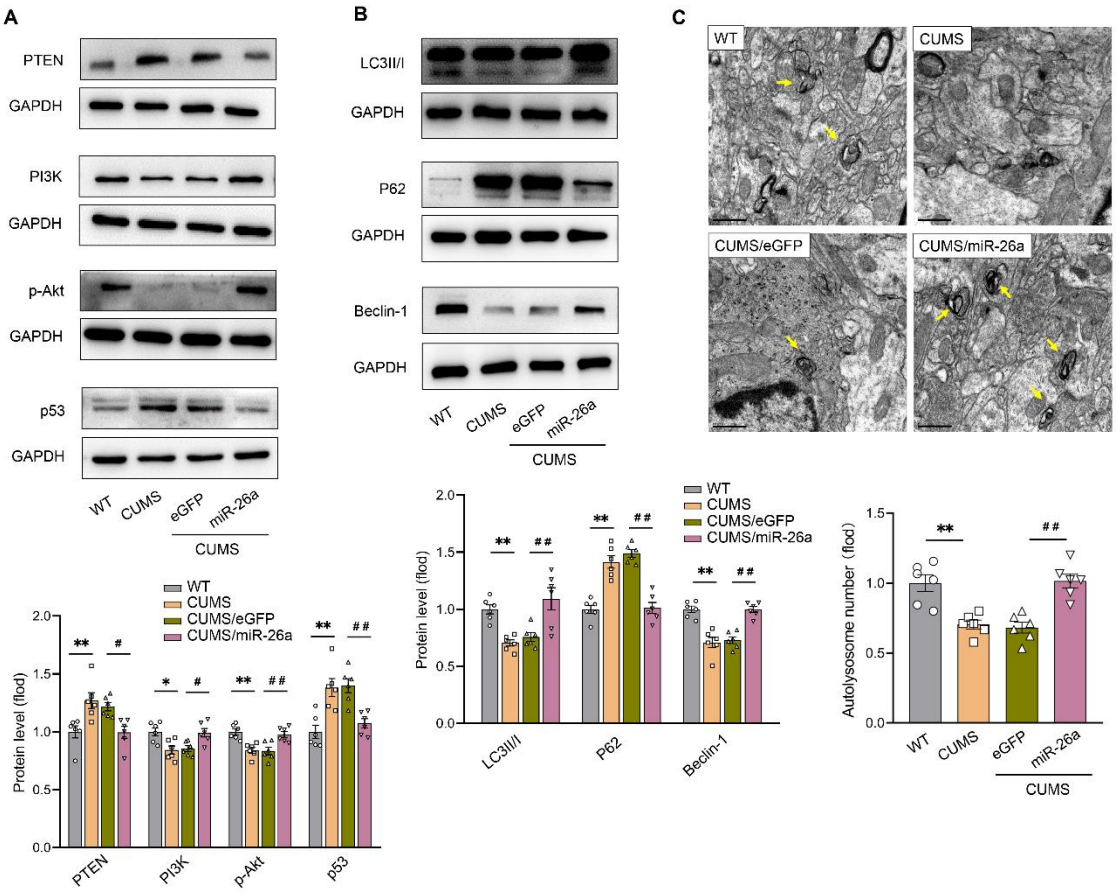

Figure. 8. Overexpression of miR-26a-3p in the DG of CUMS rats restored the attenuation in autophagy resulting from CUMS exposure. **(A)** Overexpression of miR-26a-3p in CUMS rats decreased expressions of PTEN and p53 and increased expressions of PI3K and phosphorylated Akt within the DG. N = 6 rats per group. **(B)** Overexpression of miR-26a-3p increased expressions of the LC3-II/I ratio and Beclin-1expression and decreased expressions of p62 in CUMS rats. N = 6 rats per group. **(C)** Overexpression of miR-26a-3p in the DG of CUMS rats increased the number of autolysosomes. Scale bar = 500 nm. N = 6 rats per group with at least 20 micrographs from 1 animal. Experiments performed

in triplicate with 3 biological replicates for all panels. Data are presented as the means ± SEM. *$P < 0.05$, **$P < 0.01$ vs. WT; $^{\#}P < 0.05$, $^{\#\#}P < 0.01$ vs. eGFP control (CUMS+ AAV-eGFP) by ANOVA with Tukey post hoc correction. WT, wide type.

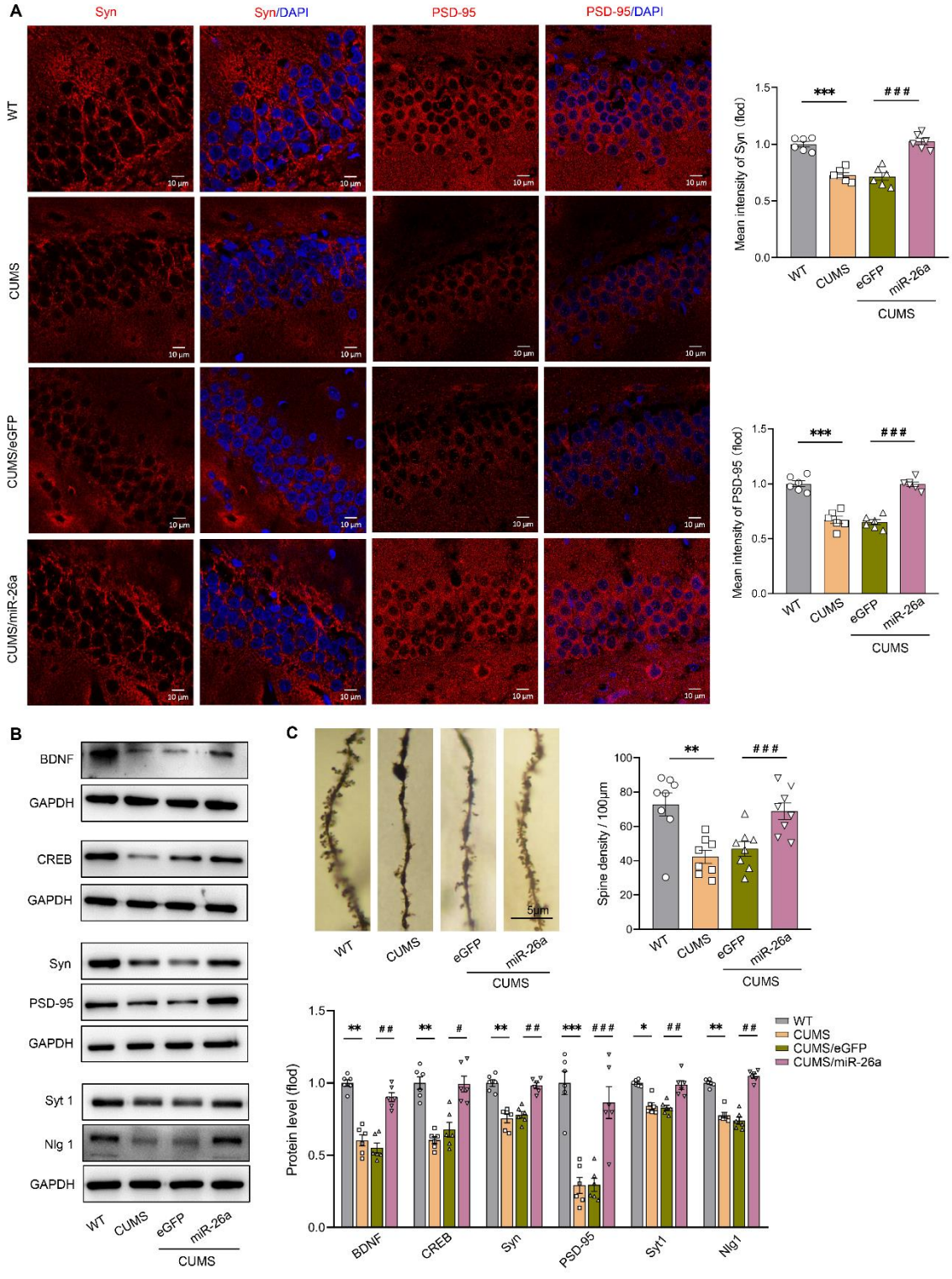
A
Syn
Syn/DAPI
PSD-95
PSD-95/DAPI
WT
CUMS
CUMS/eGFP
CUMS/miR-26a
10 μm
Mean intensity of Syn (flod)
Mean intensity of PSD-95 (flod)
***
###
WT
CUMS
eGFP
miR-26a
CUMS
B
BDNF
GAPDH
CREB
GAPDH
Syn
PSD-95
GAPDH
Syt 1
Nlg 1
GAPDH
WT
CUMS
eGFP
miR-26a
CUMS
C
5μm
Spine density / 100μm
**
###
Protein level (flod)
BDNF
CREB
Syn
PSD-95
Syt1
Nlg1
WT
CUMS
CUMS/eGFP
CUMS/miR-26a

Figure. 9. Overexpression of miR-26a-3p in the DG of CUMS rats restored the dysregulation of neuroplasticity resulting from CUMS exposure. **(A)** Representative confocal microscopic images showing the expression levels of Syn andPSD-95within the DG. Scale bar = 10μm. N = 6 rats per group and at least 4-6 images from 1 animal. **(B)** Overexpression of miR-26a-3p increased protein levels of neuroplasticity-related mediators in CUMS rats. N = 6 rats per group. Blot results were from the same samples and run parallelly in different gels. Independent biological replicate experiments were repeated 3 times. **(C)** Representative images and summary of data showing dendritic spines in DG neurons. Scale bar = 5μm. N = 8 rats per group and at least 5 pyramidal neurons from 1 animal. Immunofluorescence and Golgi staining were repeated at least 3 times and quantitation was done for representative samples from each group. Data are presented as the means ± SEM. $^{*}P < 0.05$, $^{**}P < 0.01$, $^{***}P < 0.001$ vs. WT; $^{\#}P < 0.05$, $^{\#\#}P < 0.01$, $^{\#\#\#}P < 0.001$ vs. eGFP control (CUMS+ AAV-eGFP) by ANOVA with Tukey post hoc correction. WT, wide type.

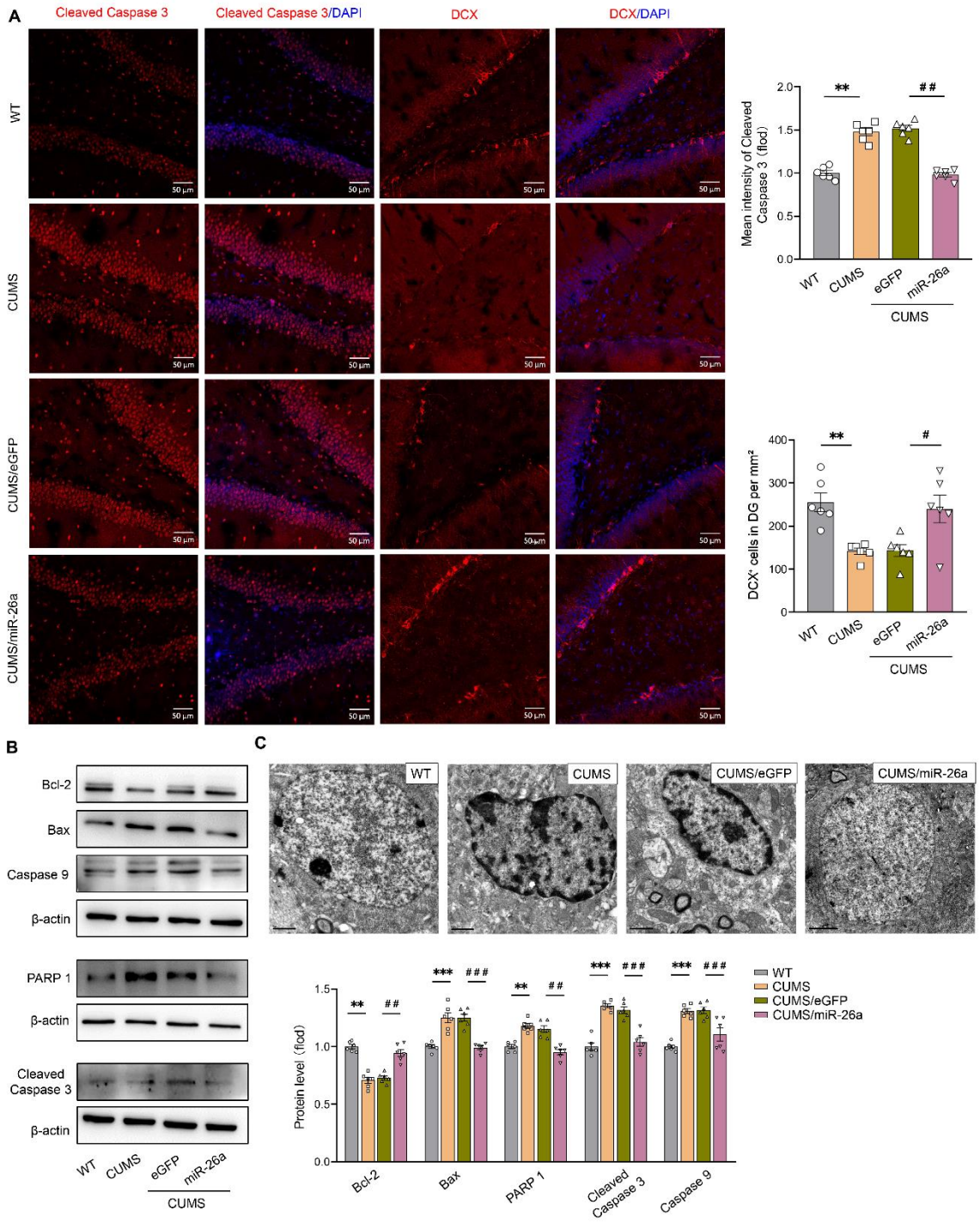

Figure. 10. Overexpression of miR-26a-3p within the DG of CUMS rats suppressed neuronal apoptosis resulting from CUMS exposure. **(A)** Representative confocal

microscopic images showing expressions of cleaved caspase-3 and DCX within the DG. Scale bar = 50μm. N = 6 rats per group and at least 4-6 images from 1 animal. **(B)** Overexpression of miR-26a-3p decreased protein levels of pro-apoptotic factors in CUMS rats. N = 6 rats per group. Blot results of Bcl-2, Bax and Caspase 9 were from the same samples and run parallelly in different gels. Independent biological replicate experiments were repeated 3 times. **(C)** Representative electronic micrographs showing nuclear chromatin abnormalities in DG neurons. Scale bar = 1 um. N= 4 rats per group and at least 20 micrographs from 1 animal. Immunofluorescence and electron microscope experiments were repeated at least 3 times and quantitation was done for representative samples from each group. Data are presented as the means ± SEM. $*P < 0.05$, $**P < 0.01$, $***P < 0.001$ vs. WT; $^{\#}P < 0.05$, $^{\#\#}P < 0.01$, $^{\#\#\#}P < 0.001$ vs. eGFP control (CUMS+ AAV-eGFP) by ANOVA with Tukey post hoc correction. WT, wide type.

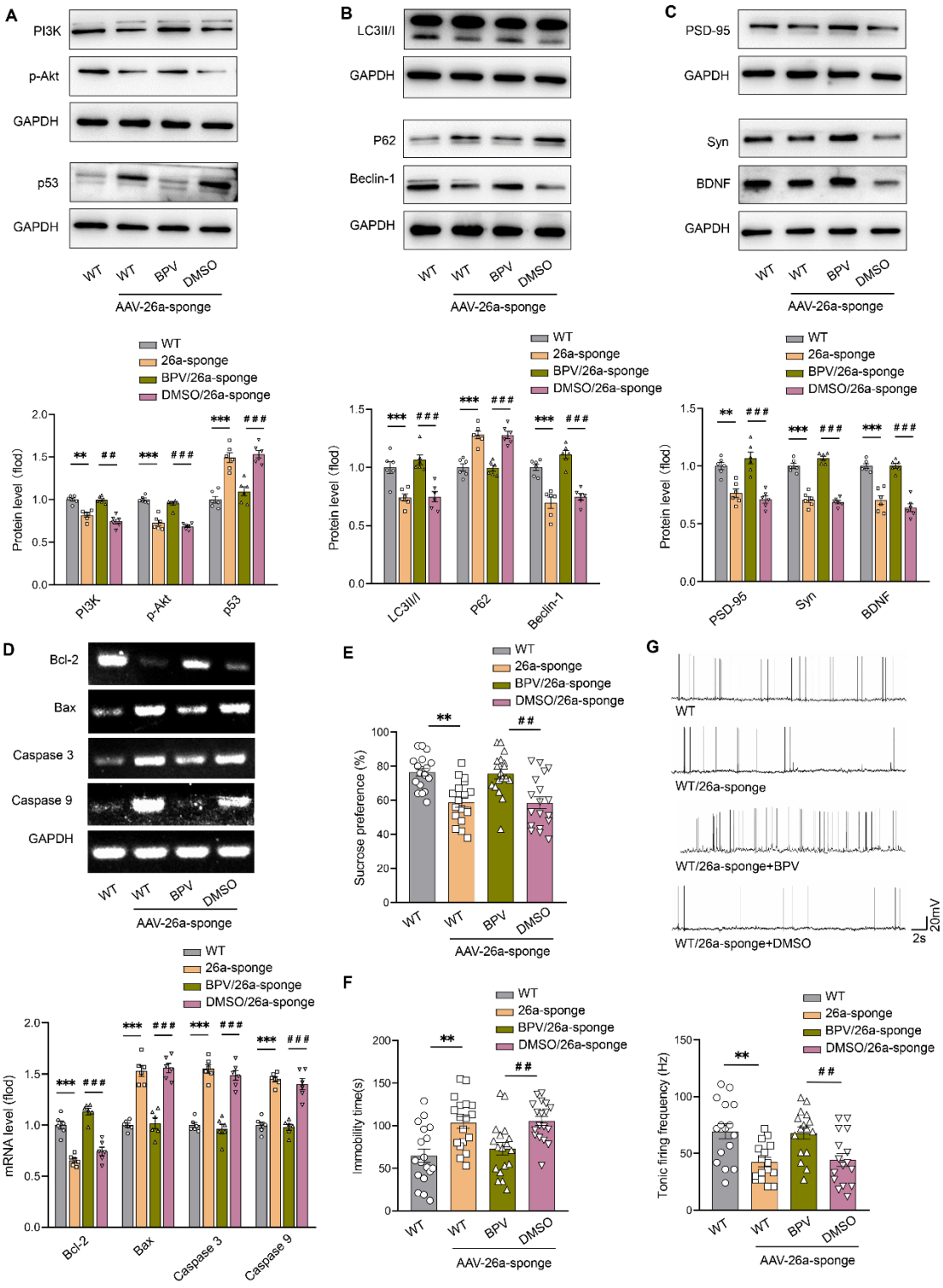
A
PI3K
p-Akt
GAPDH
p53
GAPDH
WT
WT
BPV
DMSO
AAV-26a-sponge
B
LC3II/I
GAPDH
P62
Beclin-1
GAPDH
C
PSD-95
GAPDH
Syn
BDNF
GAPDH
WT
26a-sponge
BPV/26a-sponge
DMSO/26a-sponge
Protein level (flod)
PI3K
p-Akt
p53
LC3II/I
P62
Beclin-1
PSD-95
Syn
BDNF
D
Bcl-2
Bax
Caspase 3
Caspase 9
GAPDH
mRNA level (flod)
E
Sucrose preference (%)
F
Immobility time(s)
G
WT
WT/26a-sponge
WT/26a-sponge+BPV
WT/26a-sponge+DMSO
20mV
2s
Tonic firing frequency (Hz)

Figure. 11. PTEN inhibition attenuated neuronal and behavioral anomalies resulting from miR-26a-3p deficits in the DG. **(A)** BPV (pic) treatment increased expressions of PI3K and phosphorylated Akt and decreased p53 expression levels in miR-26a-3p knock-down rats. Blot results of PI3K and p-Akt were from the same samples and run parallelly in different gels. N = 6 rats per group with 3 independent biological replicate experiments. **(B)** BPV (pic) treatment increased expression of the LC3-II/I ratio and Beclin-1, and decreased expressions of p62 in miR-26a-3p knock-down rats. Blot results of p 62 and Beclin-1were from the same samples and run parallelly in different gels. N = 6 rats per group with 3 independent biological replicate experiments. **(C)** BPV (pic) treatment increased protein levels of BDNF, PSD-95 and Syn within the DG of miR-26a-3p knock-down rats. Blot results of Syn and BDNF were from the same samples and run parallelly in different gels. N = 6 per rats group with 3 independent biological replicate experiments. **(D)** BPV (pic) treatment decreased mRNA levels of Bax, caspase 3 and caspase 9, and increased Bcl-2 mRNA levels in miR-26a-3p knock-down rats. N = 6 rats per group with 3 independent biological replicate experiments. **(E)** BPV (pic) treatment in miR-26a-3p knock-down rats increased sucrose consumption in the sucrose preference test and **(F)** decreased immobility times and increased swimming times in the forced swim test. **(G)** BPV (pic) treatment in DG neurons produced changes of spontaneous burst activity. N = 16 rats per group. Each data point represents 1 animal. Electrophysiological recording was repeated at least 3 times.

Data are presented as the means ± SEM. N = 18 rats per group in behavioral tests. *P < 0.05, **P < 0.01, ***P < 0.001 vs. WT; $^{\#}P$ < 0.01, $^{\#\#}P$ < 0.01, $^{\#\#\#}P$ < 0.001 vs. AAV-26a-sponge (WT+ AAV-miR-26a-sponge) by ANOVA with Tukey post hoc correction. WT, wide type.